TUMOR IMMUNOLOGY

Lack of CD8$^+$ T cell effector differentiation during priming mediates checkpoint blockade resistance in non–small cell lung cancer

Brendan L. Horton[1], Duncan M. Morgan[1,2], Noor Momin[1,3], Maria Zagorulya[1,4], Elen Torres-Mejia[1], Vidit Bhandarkar[1,4], K. Dane Wittrup[1,2,3], J. Christopher Love[1,2,5], Stefani Spranger[1,4,5]*

In non–small cell lung cancer (NSCLC), response to immune checkpoint blockade (ICB) is associated with programmed cell death ligand 1 expression that is induced by interferon-γ–producing, tumor-infiltrating CD8$^+$ T cells. However, not all tumors with a CD8$^+$ T cell infiltrate respond to ICB, and little is known about the mechanisms governing ICB resistance in T cell–infiltrated NSCLC. We used an orthotopic NSCLC mouse model to study ICB-refractory CD8$^+$ T cell responses. Single-cell RNA sequencing of the NSCLC mouse tumors revealed that lung cancer–specific tumor-infiltrating CD8$^+$ T cells exhibited clonal expansion but lacked expression of genes associated with effector and exhausted T cell responses, indicating that they underwent a differentiation program distinct from conventional T cell exhaustion. This lung cancer–specific T cell dysfunction program was established early during priming in the mediastinal lymph node and was characterized by robust proliferation but a failed up-regulation of effector and exhausted T cell characteristics. Intriguingly, CD8$^+$ T cells from patients with NSCLC expressed an analogous gene expression program, which appeared distinct from conventional T cell exhaustion. Administration of recombinant interleukin-2 (IL-2) and IL-12 was sufficient to restore effector T cell differentiation and induce control of KP lung tumors. These findings imply that a CD8$^+$ T cell differentiation trajectory, activated during T cell priming in the mediastinal lymph node, limits the response of CD8$^+$ T cells to ICB and thereby may contribute to failure of ICB in a subset T cell–infiltrated NSCLC.

INTRODUCTION

Immune checkpoint blockade (ICB) provides long-term tumor control and survival for a fraction of patients with non–small cell lung cancer (NSCLC) (*1*–*5*). A preexisting, tumor-reactive T cell infiltrate is prognostic for ICB response in most cancers (*6*–*8*). Nonsquamous NSCLC is a heterogeneous disease whose treatment is determined by driver mutations (*9*, *10*). Whereas *EGFR*-, *ALK*-, or *ROS1*-mutated tumors receive targeted small-molecule therapies that inhibit the activity of the corresponding oncogenic proteins, the remaining patients with NSCLC, dominated by *KRAS* mutations, receive ICB (*9*–*11*). Mutations that co-occur with *KRAS* play a role in shaping the T cell infiltrate (*11*, *12*). Tumors with mutations in *KRAS* and *LKB1*/*STK11* frequently lack T cell infiltration and are resistant to ICB (*11*, *12*). Tumors with mutations in both *KRAS* and *TP53* are frequently infiltrated with T cells (*11*, *12*). Yet, in T cell–infiltrated *KRAS*/*TP53*-mutant tumors, the ICB response rate is only ~35% (*11*, *12*). This discrepancy suggests that in *KRAS*/*TP53* mutant NSCLC, not all tumor-infiltrating T cells respond to ICB, and a better understanding of the functional states of tumor-reactive T cells is needed.

That the functional state of antitumor T cells determines ICB response is supported by clinical reports correlating programmed cell death ligand 1 (PD-L1) expression to ICB outcome in NSCLC (*3*). PD-L1 expression within the tumor microenvironment (TME) is indicative of T cell function because PD-L1 is induced by the effector cytokine interferon-γ (IFN-γ) (*13*). Patients with PD-L1–positive, T cell–infiltrated tumors comprise about 40% of the ICB-treated patients with NSCLC and are the group most likely to respond to ICB (*3*, *9*, *14*). In contrast, patients with NSCLC with PD-L1–negative, T cell–infiltrated tumors respond poorly to ICB. Clinically, these T cell responses were described as "nonfunctional," referring to their inability to produce IFN-γ (*3*). However, our understanding of the resistance mechanisms in T cell–infiltrated, ICB-refractory patients is limited.

To better understand ICB resistance in T cell–infiltrated NSCLC, we used an orthotopic model for NSCLC derived from an autochthonous genetically engineered mouse model driven by *Kras*^{G12D} expression and deletion of *Tp53* (KP cell line) (*15*). We found that antitumor T cell responses in this model entered into a T cell dysfunctional state that was distinct from T cell exhaustion (T_{ex}). This dysfunctional state shared aspects of T cell responses found in ICB-refractory, T cell–infiltrated patients with NSCLC, including a lack of up-regulation of effector molecules after ICB (*3*). We found that the functional state of the tumor-infiltrating T cell response was determined during priming in the tumor-draining lymph node (TdLN) in our model system. ICB-refractory T cell responses were characterized by a lack of effector and exhaustion molecule expression despite robust T cell activation and migration into the KP tumors. Understanding how ICB-refractory T cell responses differ from ICB-sensitive, conventionally exhausted T cell responses is of high clinical interest. An improved understanding of the impact of T cell states on antitumor immunity will enable the development of targeted therapies to engage all T cell subsets in NSCLC.

RESULTS

ICB resistance in KP lung tumors despite a brisk T cell infiltrate

We inoculated KP tumor cells intravenously to establish lung tumors or subcutaneously to establish flank tumors and subsequently administered anti–cytotoxic T lymphocyte–associated protein 4

[1]Koch Institute for Integrative Cancer Research, MIT, Cambridge, MA, USA. [2]Department of Chemical Engineering, MIT, Cambridge, MA, USA. [3]Department of Biological Engineering, MIT, Cambridge, MA, USA. [4]Department of Biology, MIT, Cambridge, MA, USA. [5]Ragon Institute of MGH, MIT, and Harvard, Cambridge, MA, USA.
*Corresponding author. Email: spranger@mit.edu

(anti–CTLA-4) and anti–PD-L1 combination ICB beginning on day 7 after tumor inoculation (Fig. 1A). KP lung tumors were unaffected by ICB (Fig. 1, B and C), but KP flank tumors had significantly delayed tumor outgrowth (Fig. 1D). Calculation of the fold change in tumor size, as a ratio of the treated tumor areas to the average of the control tumor areas, confirmed that flank tumors responded significantly better to ICB than lung tumors (Fig. 1E). Quantification of tumor-infiltrating lymphocyte (TIL) density in tumor areas using immunofluorescence (IF) staining, identified by keratin staining, confirmed that KP lung tumors had TIL (280.6 ± 29.66 T cells/mm^2, means ± SEM; Fig. 1F and fig. S1). The density of TIL in lung tumors was 29.6-fold higher compared with ICB-sensitive flank tumors (Fig. 1, F and G), indicating that ICB resistance was not driven by a lack of T cell infiltration. However, TIL in lung tumors expanded only 1.4-fold, whereas the density of TIL in flank tumors increased 11-fold after ICB (Fig. 1, F to H). This model system allowed us to gain insights into ICB resistance by contrasting ICB-resistant and ICB-sensitive T cell responses in T cell–infiltrated NSCLC driven by the same oncogenic mutations.

TIL from KP lung tumors do not exhibit conventional T_{ex}

We performed single-cell RNA sequencing (scRNA-seq) on TIL (*16*). All analyses excluded circulating CD45$^+$ cells using intravenous injection of a phycoerythrin (PE)–labeled anti-CD45 antibody before euthanasia, followed by magnetic depletion of PE-labeled cells. We sequenced 122,554 cells from eight flank and eight lung tumor–bearing mice on day 14 with and without ICB, including 10,774 T cells (Fig. 2A) and identified nine distinct T cell phenotypes (Fig. 2, B and C). Cluster proportions were not significantly different between control and ICB (fig. S2A) but were present at different proportions between sites of tumor growth (Fig. 2D). We focused our subsequent analysis on the two non-naïve CD8$^+$ T cell clusters (CD8$^+$ c1 and CD8$^+$ c2) (*6*, *17*, *18*). CD8$^+$ c1 were dominant in flank TIL, whereas CD8$^+$ c2 were dominant in lung TIL (Fig. 2, A, B, and D). CD8$^+$ c1 had increased *Pdcd1*, *Lag3*, *Tnfrsf9*, *Tnfrsf4*, *Havcr2*, *Cd160*, and *Nrgn* gene expression, all associated with conventional T cell activation and exhaustion (Fig. 2E and table S1) (*19*–*22*). CD8$^+$ c2 had higher expression of transcripts associated with CD8$^+$ T cell activation, including *Klrg1* and *Ccl5*, and T cell survival and tissue homing, including *Klf2*, *Klf3*, *S1pr1*, *S1pr4*, *Itga4*, and *Itgb1* (Fig. 2E) (*23*–*31*). Pathway analysis suggested interleukin-2 (IL-2)/signal transducer and activator of transcription 5 signaling to be enriched in CD8$^+$ c1 (Fig. 2F, fig. S2B, and table S2). These data suggested that two distinct CD8$^+$ T cell responses were induced against the KP tumor cell line depending on the location of the tumor growth; CD8$^+$ T cell responses against flank tumors were characterized by effector function and conventional T_{ex}, whereas CD8$^+$ TIL in lung tumors lacked exhaustion molecules but expressed a distinct set of effector molecules.

Flow cytometry on TIL from lung or flank tumors was performed to validate differentially expressed genes (DEGs). Lung and flank TIL expressed programmed cell death 1 (PD-1), indicative of antigen recognition occurring at both tumor sites (Fig. 2G) (*32*). Flank TIL had higher expression of molecules associated with T_{ex}: LAG-3 (*Lag3*) and 4-1BB

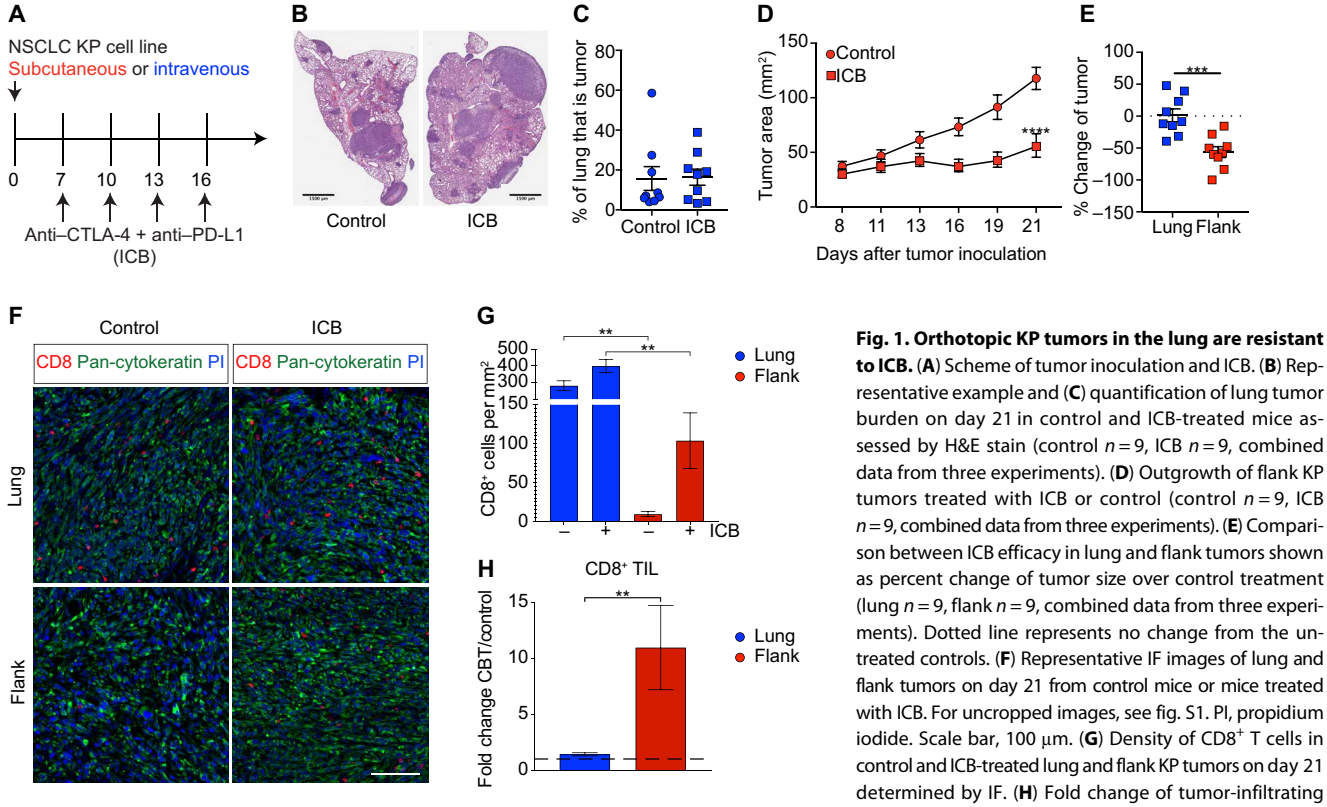

Fig. 1. Orthotopic KP tumors in the lung are resistant to ICB. (**A**) Scheme of tumor inoculation and ICB. (**B**) Representative example and (**C**) quantification of lung tumor burden on day 21 in control and ICB-treated mice assessed by H&E stain (control $n = 9$, ICB $n = 9$, combined data from three experiments). (**D**) Outgrowth of flank KP tumors treated with ICB or control (control $n = 9$, ICB $n = 9$, combined data from three experiments). (**E**) Comparison between ICB efficacy in lung and flank tumors shown as percent change of tumor size over control treatment (lung $n = 9$, flank $n = 9$, combined data from three experiments). Dotted line represents no change from the untreated controls. (**F**) Representative IF images of lung and flank tumors on day 21 from control mice or mice treated with ICB. For uncropped images, see fig. S1. PI, propidium iodide. Scale bar, 100 μm. (**G**) Density of CD8$^+$ T cells in control and ICB-treated lung and flank KP tumors on day 21 determined by IF. (**H**) Fold change of tumor-infiltrating CD8$^+$ T cells between ICB-treated and control mice. Dashed line is at 1, which is no change from the control. Regions analyzed in (G) and (H): flank, $n = 12$ from three mice; flank + ICB, $n = 14$ from four mice; lung, $n = 58$ from three mice; and lung + ICB, $n = 73$ from four mice. Data are shown as means ± SEM, and statistical analysis was conducted using a two-way ANOVA (D), MWU test (C, E, and H), or one-way ANOVA (G) with $^{**}P < 0.01$, $^{***}P < 0.001$, and $^{****}P < 0.0001$.

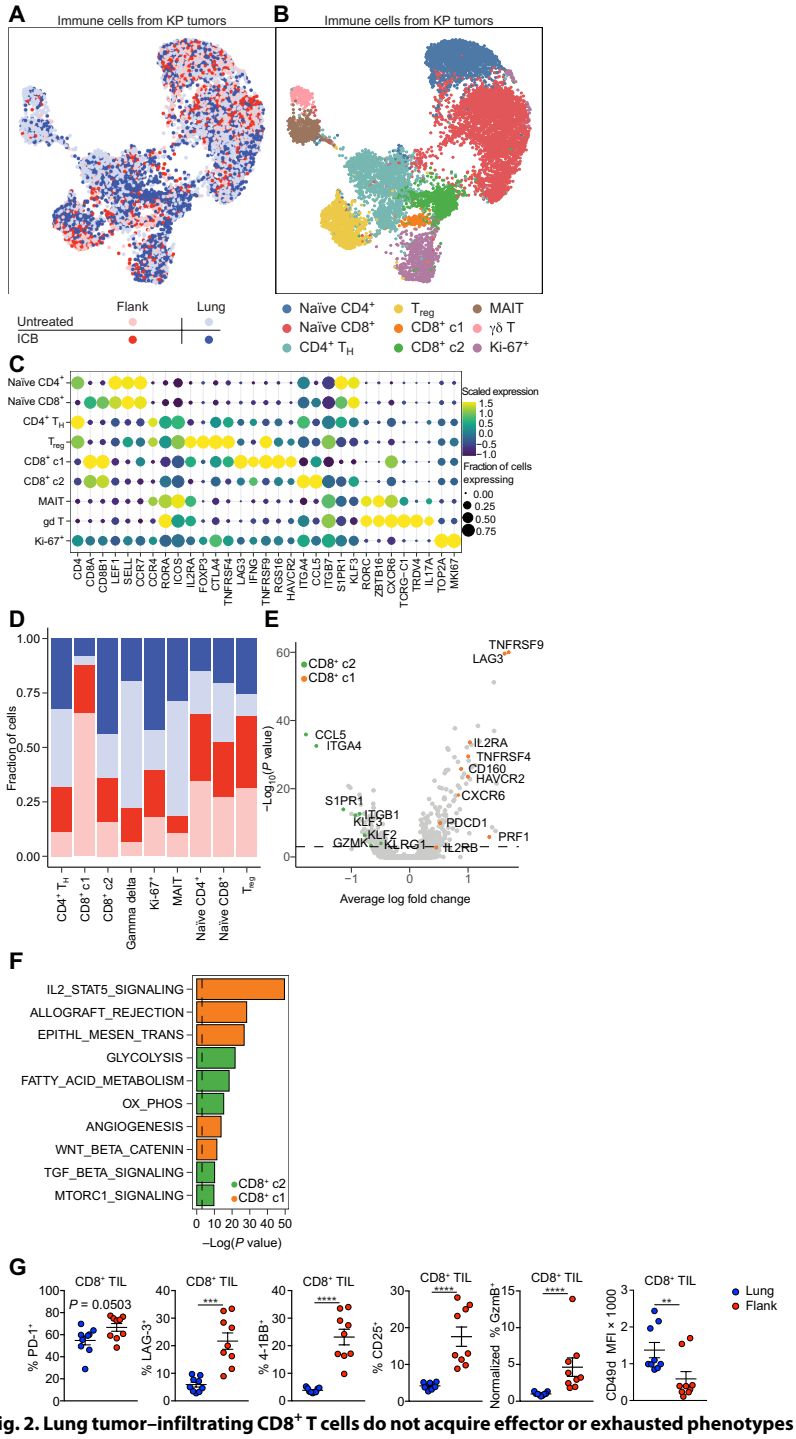

Fig. 2. Lung tumor–infiltrating CD8$^+$ T cells do not acquire effector or exhausted phenotypes observed in flank TIL. (**A**) UMAP plots of scRNA-seq indicating treatment status and tumor location and (**B**) curated clusters. T_H, T helper. MAIT, mucosal associated invariant T cell. (**C**) Bubble plot of gene expression analysis of curated clusters. (**D**) Stack charts of contributions to each curated cluster based on treatment condition and tumor location. (**E**) Volcano plot of DEGs between CD8$^+$ c1 and CD8$^+$ c2 CD8$^+$ T cells. Selected DEGs in CD8$^+$ c2 (green) or CD8$^+$ c1 (orange) TIL are highlighted. (**F**) Pathway analysis of DEGs showing enriched MSigDb hallmarks pathways for CD8$^+$ c2 (green) and CD8$^+$ c1 (orange) TIL. (**G**) Validation of differentially expressed key effector/exhaustion markers on lung and flank CD8$^+$ TIL (lung, $n = 9$ and flank, $n = 9$, combined data from three experiments). Data are shown as means ± SEM, and statistical analysis was conducted using an MWU test (G) with $^{**}P < 0.01$, $^{***}P < 0.001$, and $^{****}P < 0.0001$, or as indicated in Materials and Methods (A to F). MFI, mean fluorescence intensity.

(*Tnfrsf9*), effector T cell differentiation, CD25 (*Il2ra*), and granzyme B (*Gzmb*) (Fig. 2G), whereas CD49d (*Itga4*) was higher on lung TIL (Fig. 2H). A second model of lung cancer (LL/2) provided similar results (fig. S2C). See fig. S2D for example flow cytometry plots. Thus, in our model, lung tumor TIL exhibited signs of T cell activation yet lacked hallmarks of effector T cell differentiation and T_{ex}. We therefore concluded that lung tumor–reactive TIL in our models were in a dysfunctional state distinct from T_{ex}. For ease, we refer to this T cell state as lung cancer–specific T cell dysfunction, abbreviated T_{Ldys}, throughout the manuscript.

TIL with T_{Ldys} are tumor antigen specific

Differences in TIL between lung and flank KP tumors could be driven by differences in antigen specificities or T cell receptor (TCR) usage. We recovered *Tcra* and *Tcrb* sequences from single-cell libraries (*33*). CD8$^+$ c1 and CD8$^+$ c2 both showed clonal expansion in lung and flank KP tumors, suggesting that both sites of tumor growth induced a tumor-reactive T cell response (fig. S2E). Using grouping of lymphocyte interactions by paratope hotspots 2 (GLIPH2) (*34*) to analyze similarities in the TCR repertoire, we identified seven specificity groups that contained CDR3 sequences from three or more mice and that were shared across flank and lung tumors and both CD8$^+$ phenotypes (fig. S2F). Identification of public clonotypes suggests a shared antigen present in both lung and flank KP tumors (table S3) capable of inducing clonal expansion.

To directly determine whether CD8$^+$ T cell responses against the same antigen could enter the CD8$^+$ c1 and CD8$^+$ c2 states, we engineered KP cells to express the model antigen SIYRYYGL (SIY, KP.SIY cell line), which is presented on H-2K^b. Using SIY-loaded pentamers, we sorted SIY-reactive CD8$^+$ TIL from day 14 lung and flank KP.SIY tumors. To elucidate whether SIY-reactive CD8$^+$ T cells were transcriptionally similar to CD8$^+$ T cell populations from KP parental lung and flank tumors, we conducted an integrated analysis of both datasets. We determined a high degree of overlap in the clustering of lung and flank SIY-reactive CD8$^+$ TIL with their respective counterparts from KP parental tumors (Fig. 3A). Unsupervised analysis of the integrated data yielded two clusters consistent with the CD8$^+$ c1 and CD8$^+$ c2 in the KP parental cell line (Fig. 3B). The proportion of CD8$^+$ c1 and CD8$^+$ c2 within TIL from KP.SIY and KP parental tumors was similar (Fig. 3C), with CD8$^+$ c1 being 47 and 59% of KP and KP.SIY flank TIL, respectively. Lung TIL consisted of 90 and 89% CD8$^+$ c2 from KP and KP.SIY tumors, respectively, demonstrating that the T_{Ldys} phenotype is dominant in lung TIL (Fig. 3C). Next, we determined the DEGs between CD8$^+$ c1 and CD8$^+$ c2 from the KP.SIY TIL (Fig. 3D and table S4). Consistently, CD8$^+$ c1 from KP.SIY tumors had higher expression of exhaustion markers, including *Tnfrsf9*, *Tnfrsf4*, *Lag3*, *Cd160*, and *Havcr2*, whereas CD8$^+$ c2 had higher expression of lung-homing factors, including *Ccl5* and *Itga4*. A comparison of DEGs between CD8$^+$ c1 and CD8$^+$ c2 from

both the KP parental and KP.SIY CD8$^+$ TIL datasets showed a highly significant degree of similarity ($R = 0.55$, $P < 0.001$; Fig. 3E), indicating that the transcriptional differences between CD8$^+$ c1 and CD8$^+$ c2 were conserved in TIL isolated from KP parental and KP.SIY tumors. This suggested that T_{Ldys} (CD8$^+$ c2) was not a result of weak or absent reactivity to tumor-associated antigens because T cell responses against SIY induced differentiation to this T cell state.

Flow cytometric analysis of SIY-reactive TIL (Fig. 3F) confirmed that the phenotypes of lung and flank TIL were similar to those observed in KP parental tumors (Figs. 2G and 3F). We also performed intratracheal administration of KP.SIY cells as a second method of tumor inoculation into the lung. We detected a difference in only CD49d between intravenously and intratracheally induced lung tumors, suggesting that intravenous tumor inoculation was not driving T_{Ldys} (Fig. 3F). In summary, differences between lung and flank TIL were preserved in the presence of a strong neoantigen and were consistent between intravenous and intratracheal lung tumor induction.

T_{Ldys} is not driven by the lung TME

Because separation of tumors from normal lung tissue before analysis was not feasible, we used IF staining to determine whether T_{Ldys} T cells were in the TME or within the adjacent lung. Using keratin to identify tumor areas, we found that CD8$^+$ T cells were significantly enriched in lung tumors compared with the adjacent normal tissue

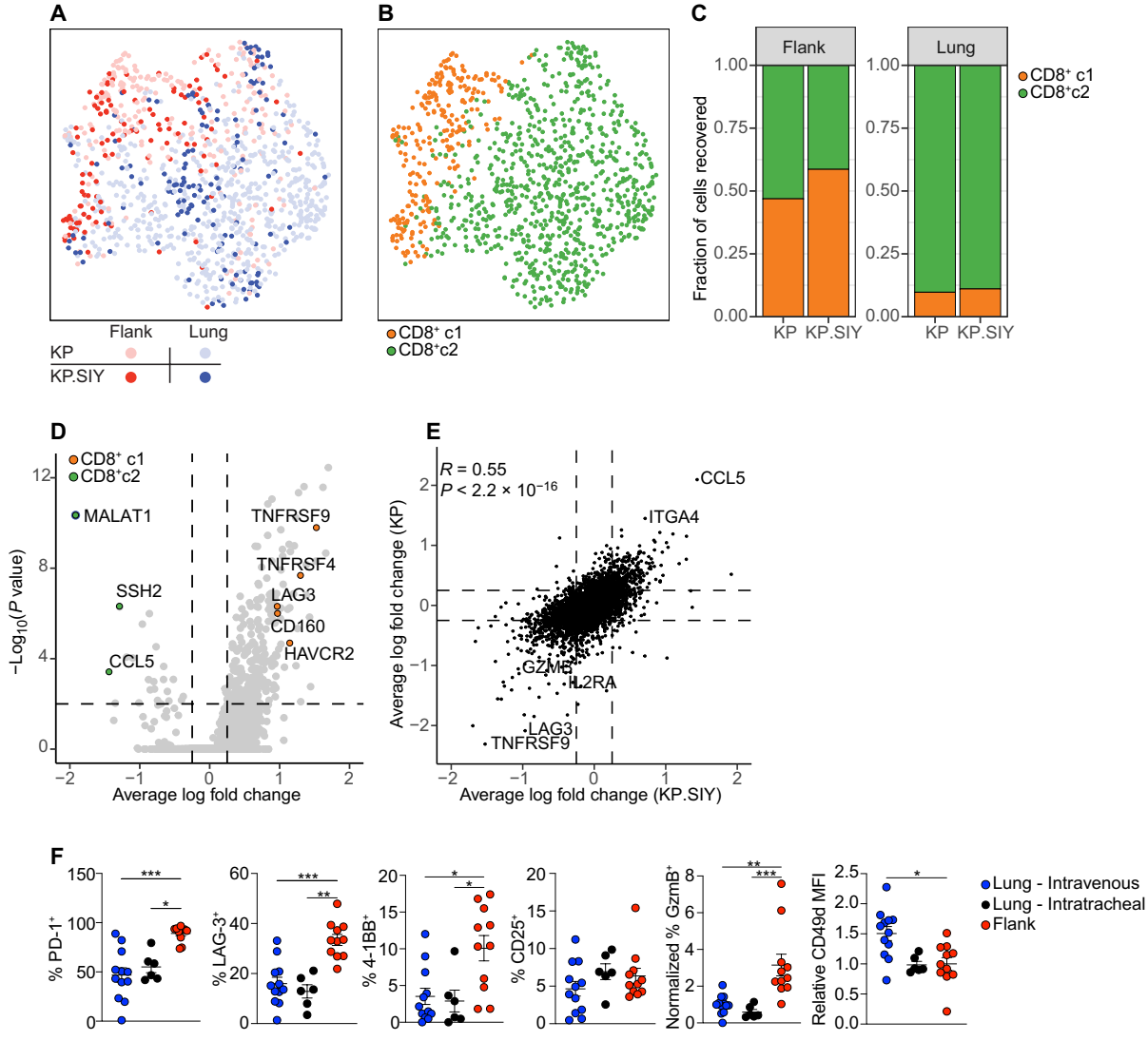

Fig. 3. T_{Ldys} T cells in lung tumors and T_{ex} T cells in flank tumor respond to the same antigen. (**A**) Combined UMAP plot of scRNA-seq of polyclonal CD8$^+$ T cells (lung and flank KP tumors) and SIY-pentamer$^+$ CD8$^+$ T cells (lung and flank KP.SIY tumors) indicating tumor cell line and location. (**B**) UMAP plot showing clusters CD8$^+$ c1 and CD8$^+$ c2 of combined datasets from (A). (**C**) Proportions of cluster CD8$^+$ c1 or CD8$^+$ c2 within flank and lung TIL. (**D**) Volcano plot of DEGs between CD8$^+$ c1 and CD8$^+$ c2 SIY-reactive CD8$^+$ T cells. Genes of interest are highlighted. (**E**) The log fold change values of DEGs between CD8$^+$ c1 and CD8$^+$ c2 were compared between SIY-reactive CD8$^+$ T cells from KP.SIY tumors and polyclonal CD8$^+$ T cells from KP tumors. (**F**) Flow cytometry of SIY-reactive TIL from KP.SIY lung and flank tumors (lung intravenous, $n = 12$; lung intratracheal, $n = 6$; and flank $n = 11$; data pooled from four independent experiments, two with intratracheal tumor administration). Data are shown as means ± SEM, and statistical analysis was conducted using an MWU test (F) with *$P < 0.05$, **$P < 0.01$, and ***$P < 0.001$, or as indicated in Materials and Methods (A to E).

(fig. S3, A and B). This was true for lung tumors inoculated intravenously or intratracheally (fig. S3, A and B), indicating that most $CD8^+$ T cells from lung tumor–bearing mice resided in the tumor (see also fig. S1). We next quantified PD-1 expression on $CD8^+$ T cells infiltrating lung tumors or the adjacent normal tissue because PD-1 is expressed upon antigen encounter (*32*). PD-1^+CD8^+ T cells were significantly enriched in lung tumors compared with adjacent tissue (fig. S3, A and C). PD-1 was expressed on 74.5, 78.3, and 73.7% of $CD8^+$ T cells from intravenous lung, intratracheal lung, and flank tumors, respectively (fig. S3, A and D). These data indicate that most PD-1^+ $CD8^+$ T cells are within tumors and suggest that the differences between T_{ex} and T_{Ldys} TIL are not due to failed infiltration of TIL with T_{Ldys} into the tumor.

To further determine whether T_{Ldys} were independent of the lung TME, we adoptively transferred 20,000 Thy1.2^+ fluorescence-activated cell sorting (FACS)–sorted TIL from flank or lung tumors into Rag$2^{-/-}$ mice. Eight to 16 weeks later, we inoculated the reconstituted Rag$2^{-/-}$ mice with KP flank tumors. Adoptively transferred TIL from KP flank tumors led to slower tumor growth compared with those from KP lung tumors (fig. S3E), suggesting that TIL from KP lung and flank tumors are functionally different and that T_{Ldys} is a persistent T cell state that cannot be reversed by a flank tumor or homeostatic proliferation.

To probe for earlier differences in T cell responses against lung and flank tumors, we performed a concomitant immunity assay. Mice bearing flank or lung KP tumors were challenged with a second KP tumor implanted on the contralateral flank 7 days after the first tumor inoculation. Mice bearing an initial flank tumor experienced significantly improved tumor control of the second tumor compared with naïve mice (fig. S3F), but mice with an initial lung tumor showed no protection against a second flank tumor (fig. S3F). Similar results were obtained with the KP.SIY cell line (fig. S3G). Antibody-mediated depletion confirmed that this protection was due to $CD8^+$ T cells (fig. S3H). To determine whether the lung TME was sufficient to induce T_{Ldys} after initial T cell activation, we assessed the effect of an initial flank tumor on the growth of subsequent lung tumors and observed protection against a second lung tumor challenge (fig. S3I), suggesting that the lung TME was not directly imposing T_{Ldys}. These data suggest that the T_{Ldys} induced by KP and LL/2 lung tumors is a persistent state of T cell dysfunction established early during the anti–lung tumor immune response.

T_{Ldys} is established during T cell priming in the mediastinal LN

We next postulated that the differences in $CD8^+$ T cell responses were imposed during T cell priming in the lung tumor–draining mediastinal LN (mLN) or flank tumor–draining inguinal LN (iLN). To determine whether differences in antitumor T cell responses could be detected in the periphery, we performed an IFN-γ enzyme-linked immune absorbent spot (ELISpot) assay. KP lung tumors had significantly fewer IFN-γ–producing, SIY-reactive splenocytes compared with KP flank tumors (fig. S4A). To determine whether this was due to a lack of T cell proliferation during priming, we used an adoptive T cell transfer approach using TCR-transgenic 2C T cells (2C T cells) specific for SIY (*35*). Naïve, carboxyfluorescein diacetate succinimidyl ester (CFSE)–labeled 2C T cells were transferred into mice with KP.SIY lung or flank tumors on day 7, and the degree of T cell activation was determined in TdLN on day 10. The 2C T cells proliferated robustly in both the mLN and the iLN (fig. S4, B and C), suggesting that differences in antitumor $CD8^+$ T cell responses were not due to a lack of T cell expansion during priming.

Next, we adoptively transferred 2C T cells to mice with KP.SIY lung or flank tumors on day 7. On day 10, 2C T cells from the mLN of lung tumor–bearing mice and the iLN of flank tumor–bearing mice were isolated using FACS, and scRNA-seq was performed using Smart-Seq to determine transcriptional differences between 2C T cells primed in the mLN or iLN (Fig. 4A). A total of 1744 genes were differentially expressed between 2C T cells priming in iLN or mLN (table S5). Consistent with the scRNA-seq data of endogenous flank TIL, 2C T cells primed in iLN showed high levels of genes associated with effector function (*Gzma*, *Gzmb*, *Il2ra*, *Il12rb1*, *Il12rb2*, *Prdm1*, *Bhlhe40*, and *Id2*) (*36*–*39*) and exhaustion (*Pdcd1*, *Havcr2*, *Tnfrsf4*, and *Cd160*) (*19*–*22*) (Fig. 4B). In contrast, 2C T cells primed in the mLN showed high levels of genes associated with inhibition of effector T cell differentiation (*Sell*, *Pecam1*, *Bcl6*, *Id3*, *Lef1*, *Ctla4*, *Bach2*, *Tox*, and *Tox2*) (*36*–*44*) and genes associated with lung T cell responses (*Ccl5*, *Itga4*, and *Itgb1*) (*23*–*25*) (Fig. 4B). Direct comparison of 2C T cells and endogenous $CD8^+$ TIL revealed that 42 genes were consistently regulated between these early and late $CD8^+$ T cell responses (fig. S4D and table S6), suggesting that differences in T cell responses between lung and flank KP tumors originated from differences during T cell priming. Flow cytometry affirmed that CD25 and GzmB were significantly reduced on T cells activated in mLN (Fig. 4, C and D), whereas mLN-primed 2C T cells showed higher levels of CD49d (Fig. 4E).

To determine whether differences in antigen-presenting cells (APCs) in the TdLN were responsible for the differences in T cell priming, we examined tumor antigen–containing APC using KP tumor cells engineered to express ZsGreen, allowing extended detection of APC populations carrying tumor cell debris (*45*, *46*). Flow cytometry of $ZsGreen^+$ cells in the mLN of lung tumor–bearing mice and the iLN of flank tumor–bearing mice on day 7 after tumor inoculation revealed that conventional dendritic cells (DCs) were the dominant APC that acquired tumor antigen and migrated to the TdLN (fig. S4E). Furthermore, we detected equal numbers of $ZsGreen^+$ DCs in both mLN and iLN (fig. S4F). To assess functional abilities of DCs, KP cells expressing ZsGreen and the SIIN peptide were inoculated into mice, and 7 days later $ZsGreen^+$ DCs were sorted from TdLNs. $ZsGreen^+$ DCs were cocultured with naïve TCR-transgenic $CD8^+$ T cells specific for SIIN peptide (OT-I T cells). We detected identical T cell activation using $ZsGreen^+$ DCs from mLN or iLN (fig. S4G), indicating that both DC populations have similar stimulatory capacity ex vivo, highlighting that differences between $CD8^+$ T cell responses against lung and flank tumors were not due to differences in DC-mediated antigen presentation.

We next evaluated the priming of endogenous SIY-reactive T cells in response to KP.SIY lung and flank tumors. We found no significant differences in either the percentage or number of SIY-reactive $CD8^+$ T cells on day 7 after tumor inoculation (Fig. 4F). However, SIY-reactive $CD8^+$ T cells in the iLN of flank tumor–bearing mice expressed higher CD25 and GzmB (Fig. 4, G and H). SIY-reactive $CD8^+$ T cells in the mLN of lung tumor–bearing mice expressed higher Tox (Fig. 4I), consistent with higher *Tox* transcript levels in 2C T cells primed in mLN (Fig. 4B). We next assessed the T cell phenotype of SIY-reactive $CD8^+$ T cells in the mLN after intravenous or intratracheal KP tumor administration. SIY-reactive $CD8^+$ T cells in the mLN had reduced CD25 and GzmB and increased CD49d compared with SIY-reactive $CD8^+$ T cells in the iLN, indicating that these differences in priming occurred with both intravenous and intratracheal inoculation

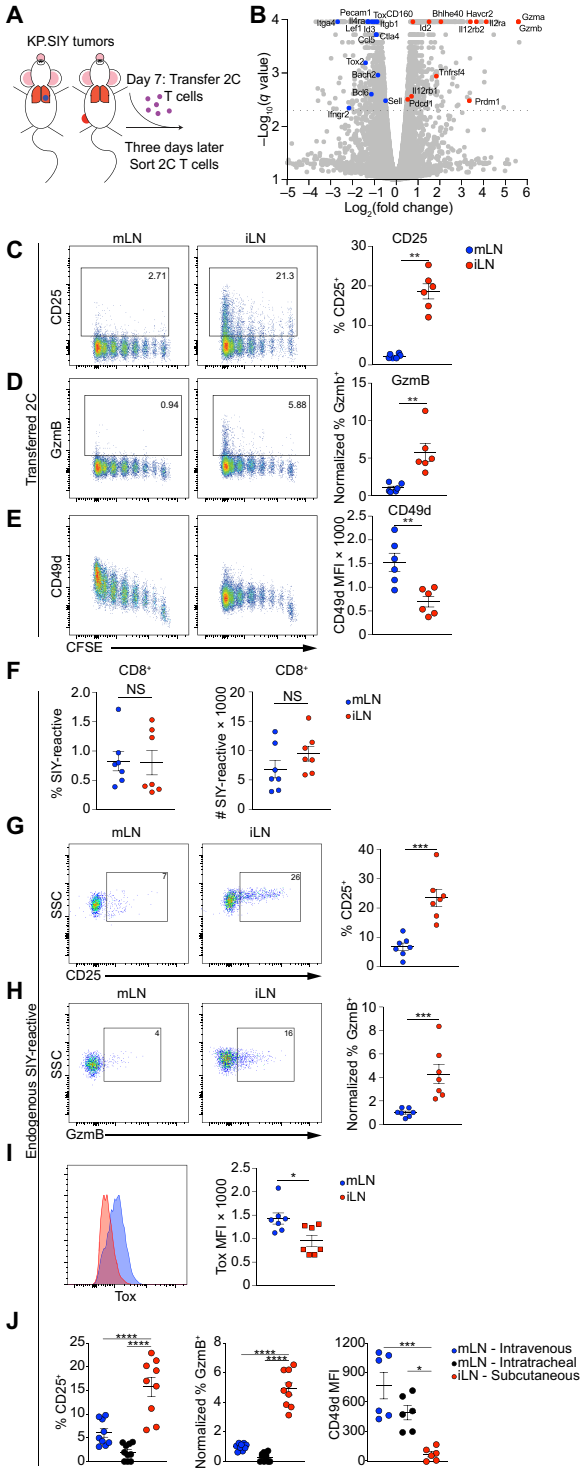

Fig. 4. CD8$^+$ T cells primed in the mLN fail to acquire an effector phenotype. (**A**) Schematic of experimental setup. Mice were inoculated with KP.SIY lung or flank tumors, and on day 7 of tumor growth, 1×10^6 naïve, congenically marked 2C T cells were transferred to tumor-bearing mice. On day 10 of tumor growth, the 2C T cells were isolated from the mLN of lung tumor–bearing mice and iLN of flank tumor–bearing mice using FACS. (**B**) Volcano plot of DEGs between 2C T cells primed in the mLN and iLN of tumor-bearing mice. mLN, $n = 3$ and iLN, $n = 4$ biological replicates. Genes of interest are highlighted. (**C** to **E**) Representative example and quantification (means ± SEM) of CD25 (C), GzmB (D), and CD49d (E) expression levels on CFSE-labeled 2C T cells primed in the mLN and iLN of tumor-bearing mice at 72 hours after adoptive transfer, day 10 of tumor growth (mLN, $n = 6$ and iLN, $n = 6$; data pooled from two experiments). CFSE dilution is shown on the *x* axis. (**F** to **I**) Representative example and quantification (means ± SEM) of the percent and absolute number of SIY$^+$-reactive T cells (F) as well as CD25 (G), GzmB (H), and Tox (I) expression levels on endogenous SIY-reactive T cells in the mLN and iLN of tumor-bearing mice 7 days after tumor inoculation. NS, not significant; SSC, side scatter. (**J**) Mice were inoculated with KP.SIY cells either intravenously, intratracheally, or subcutaneously. On day 7 of tumor growth, mLNs and iLNs were isolated, and endogenous SIY-reactive CD8$^+$ T cells were analyzed with flow cytometry for the expression of CD25, GzmB, and CD49d ($n = 9$ for CD25 and GzmB and $n = 6$ for CD49d comparisons, data pooled from three experiments). Data are shown as means ± SEM, and statistical analysis was conducted using an MWU test (C to J) with $^*P < 0.05$, $^{**}P < 0.01$, $^{***}P < 0.001$, and $^{****}P < 0.0001$ or as indicated in Materials and Methods (B).

(Fig. 4J). To determine whether these differences in T cell activation were due to the orthotopic nature of KP lung tumor, we inoculated mice with the melanoma cell line B16.SIY. Responses in the mLN were similar to responses in the iLN (fig. S5, A and B), indicating that CD8$^+$ T cell priming in the mLN in response to orthotopic tumors in the lung led to T_{Ldys}.

T cells with T_{Ldys} retain T cell factor 1 but are functionally distinct from precursor-exhausted T cells

Studies in chronic lymphocytic choriomeningitis virus (LCMV) have described two subsets of exhausted CD8$^+$ T cells: terminally exhausted T cell immunoglobulin and mucin domain-containing protein 3 (TIM-3$^+$) CD8$^+$ T cells, which gradually lose their functional properties and eventually undergo apoptosis, and precursor-exhausted T cell factor 1–positive (TCF-1$^+$) CD8$^+$ T cells that lack cytotoxicity but retain a stem-like capacity to differentiate into TIM-3$^+$ T cells (*36*, *47*). Because *Havcr2*, which encodes TIM-3, was differentially expressed on tumor-reactive CD8$^+$ T cells in mLN and iLN and the corresponding TIL populations, we determined the expression of TIM-3 and TCF-1 during CD8$^+$ T cell responses to lung and flank KP.SIY tumors. TIM-3 was up-regulated on CD8$^+$ T cells in the iLN, both on transferred 2C T cells (Fig. 5A) and on endogenous SIY-specific CD8$^+$ T cells (Fig. 5B). In contrast, CD8$^+$ T cells activated in the mLN did not up-regulate TIM-3 and remained TCF1$^+$ (Fig. 5, A and B). These differences were specific for orthotopic lung KP tumors because no differences were detected using B16.SIY tumors (fig. S5C).

We next analyzed TIL on day 14 after tumor inoculation. Both adoptively transferred 2C T cells and endogenous T cells acquired a terminally exhausted TIM-3$^+$ TCF1$^-$ phenotype in flank tumors (Fig. 5, C and D). However, neither 2C T cells nor SIY-reactive TIL in lung tumors acquired significant TIM-3$^+$ expression and remained either TCF-1$^+$ or became TIM-3$^-$ TCF-1$^-$ (Fig. 5, C and D) despite up-regulation of PD-1 (Figs. 2G and 3F and fig. S3, A, C, and D), suggesting that T cells were responding to their cognate antigen without acquiring T cell effector function. TCF-1 expression by SIY-reactive CD8$^+$ T cells in mLN and lung tumors raised the possibility that KP lung tumors had an increased proportion of precursor-exhausted CD8$^+$ T cells. Because ICB targets TCF-1$^+$ precursor-exhausted CD8$^+$ T cells and induces their differentiation into TIM-3$^+$ TCF-1$^-$ effector T cells (*37*, *40*, *48*–*51*), we determined the potential of TCF-1$^+$ T cells in mLN to differentiate to TIM3$^+$ T cells. We treated mice on days 7 and 10 of KP.SIY tumor growth with ICB and evaluated the phenotypes of SIY-reactive CD8$^+$ T cells. The proportion of TIM3$^+$ TCF1$^-$ SIY-reactive CD8$^+$ T cells in the iLN of flank tumor–bearing mice increased after

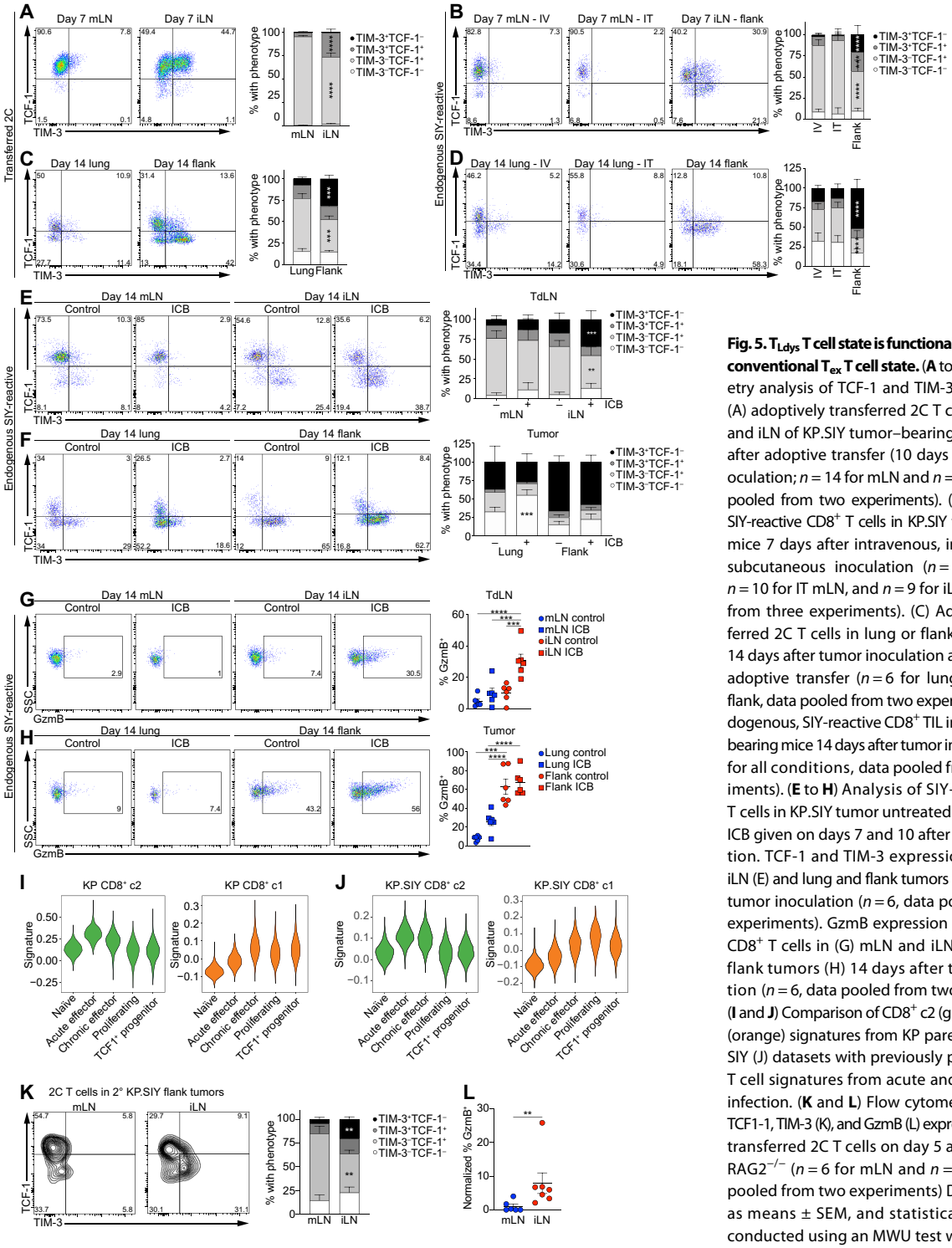

Fig. 5. T_{Ldys} T cell state is functionally distinct from conventional T_{ex} T cell state. (**A** to **D**) Flow cytometry analysis of TCF-1 and TIM-3 expression on (A) adoptively transferred 2C T cells in the mLN and iLN of KP.SIY tumor–bearing mice 72 hours after adoptive transfer (10 days after tumor inoculation; $n = 14$ for mLN and $n = 10$ for iLN, data pooled from two experiments). (B) Endogenous, SIY-reactive $CD8^+$ T cells in KP.SIY tumor–bearing mice 7 days after intravenous, intratracheal, or subcutaneous inoculation ($n = 9$ for IV mLN, $n = 10$ for IT mLN, and $n = 9$ for iLN, data pooled from three experiments). (C) Adoptively transferred 2C T cells in lung or flank KP.SIY tumors 14 days after tumor inoculation and 7 days after adoptive transfer ($n = 6$ for lung and $n = 5$ for flank, data pooled from two experiments). (D) Endogenous, SIY-reactive $CD8^+$ TIL in KP.SIY tumor–bearing mice 14 days after tumor inoculation ($n = 6$ for all conditions, data pooled from two experiments). (**E** to **H**) Analysis of SIY-reactive $CD8^+$ T cells in KP.SIY tumor untreated or treated with ICB given on days 7 and 10 after tumor inoculation. TCF-1 and TIM-3 expression in mLN and iLN (E) and lung and flank tumors (F) 14 days after tumor inoculation ($n = 6$, data pooled from two experiments). GzmB expression on SIY-reactive $CD8^+$ T cells in (G) mLN and iLN and lung and flank tumors (H) 14 days after tumor inoculation ($n = 6$, data pooled from two experiments). (**I** and **J**) Comparison of $CD8^+$ c2 (green) or $CD8^+$ c1 (orange) signatures from KP parental (I) and KP.SIY (J) datasets with previously published $CD8^+$ T cell signatures from acute and chronic LCMV infection. (**K** and **L**) Flow cytometric analysis of TCF1-1, TIM-3 (K), and GzmB (L) expression in serially transferred 2C T cells on day 5 after transfer to $RAG2^{-/-}$ ($n = 6$ for mLN and $n = 7$ for iLN, data pooled from two experiments) Data are shown as means ± SEM, and statistical analysis was conducted using an MWU test with $^{**}P < 0.01$, $^{***}P < 0.001$, and $^{****}P < 0.0001$ (A to H and K to L).

ICB, with no differences in T cell phenotype detected in the mLN of lung tumor–bearing mice (Fig. 5E). Consistent with this observation, we detected no accumulation of $TIM3^+$ $TCF1^-$ TIL in KP lung tumors; instead, ICB resulted in increased TIM-3^- TCF-1^- $CD8^+$ TIL (Fig. 5F). SIY-specific $CD8^+$ T cells in mLN and KP lung tumors also failed to up-regulate GzmB after ICB, whereas ICB enhanced GzmB expression in SIY-reactive $CD8^+$ T cells in the iLN (Fig. 5, G and H). Lack of TIM-3 and GzmB up-regulation in SIY-reactive $CD8^+$ T cells from mLN and lung tumors after ICB was consistent with the lack of ICB efficacy in KP lung tumors (Fig. 1, A to E) and suggested that the TCF-1^+ $CD8^+$ T cells in mLN and lung tumors are functionally distinct from precursor-exhausted $CD8^+$ T cells.

We compared the transcriptional profiles of TIL with a published dataset of T cell exhaustion (*36*). $CD8^+$ c2 from both the KP and KP.SIY scRNA-seq datasets, which constitutes T_{Ldys}, was most enriched for naïve and acute effector gene signatures despite low expression of effector molecules such as GzmB and CD25 (Fig. 5, I and J). $CD8^+$ c1 from both the KP and KP.SIY scRNA-seq datasets were most similar to signatures from exhausted effectors and TCF-1^+ precursor-exhausted T cells (Fig. 5, I and J). These data suggest that despite TCF-1 expression, lung tumor–reactive T_{Ldys} $CD8^+$ T cells are transcriptionally and functionally distinct from precursor-exhausted T cells. Thus, T cells with T_{Ldys} are activated and gain tissue-homing capabilities but minimally differentiate into TIM-3^+ $CD8^+$ T cells and fail to acquire appreciable effector T cell functions even when exposed to ICB.

T_{Ldys} is associated with decreased T cell functionality

To measure the functionality of the T_{Ldys} state, we assessed cytokine production from SIY-reactive TIL from KP.SIY tumors. Although neither lung nor flank TIL produced high levels of IL-2, we detected significantly lower production of tumor necrosis factor–α and IFN-γ in lung TIL compared with flank TIL (fig. S6A). To evaluate cytotoxicity, we performed an in vivo cytotoxicity assay (*52*). Flank tumor–bearing mice showed increased eradication of SIY-pulsed cells, whereas no significant cytotoxicity was detected in lung tumor–bearing animals (fig. S6B). These results demonstrated that T cells with T_{Ldys} fail to differentiate into cytotoxic effector T cells despite robust T cell activation in the mLN (Fig. 4, C to E) and successful infiltration into lung tumors (fig. S3, A to C).

To determine the persistence of the T_{Ldys} state after T cell priming, naïve 2C T cells were transferred to lung or flank KP.SIY–bearing mice on day 7, isolated from mLN or iLN on day 10, and transferred to $RAG2^{-/-}$ mice bearing flank KP.SIY tumors. The 2C T cells primed in the mLN retained a TCF-1^+ TIM-3^- phenotype with decreased GzmB after infiltration into flank tumors, whereas the 2C T cells primed in iLN retained increased TIM-3 and GzmB expression (Fig. 5, K and L). This further affirmed that T_{Ldys} is a persistent state induced during T cell priming in the mLN rather than a consequence of differential stimulation in the TME.

T_{Ldys} is detectable in patients with NSCLC

To determine whether a T_{Ldys} T cell gene signature identifies subsets of human NSCLC TIL, we generated a uniform manifold approximation and projection (UMAP) plot from a scRNA-seq study of human NSCLC (Fig. 6A) (*53*) and mapped signatures corresponding to T_{ex} and T_{Ldys} phenotypes onto this UMAP (Fig. 6B and table S7). The T_{ex} signature enriched among the terminally differentiated CD8-LAYN cluster, whereas the T_{Ldys} signature was enriched among the less differentiated CD8-KLF2 (Kruppel like factor 2), CD8-GZMK, and CD8-XCL1 clusters (Fig. 6B). Pseudotemporal ordering revealed a trajectory from the CD8-KLF2, CD8-GZMK, and CD8-XCL1 populations to the terminally differentiated CD8-LAYN phenotype (Fig. 6C). Along this trajectory, the T_{Ldys} signature was down-regulated as a function of pseudotime, whereas the T_{ex} signature was up-regulated (Fig. 6D). Thus, less differentiated $CD8^+$ T cell populations in human NSCLC demonstrated transcriptomic similarity to the T_{Ldys} T cell state found in KP lung tumors, whereas terminally exhausted $CD8^+$ T cell were closely related to the T_{ex} T cells that dominate KP flank tumors. These observations suggest that both T_{ex} and T_{Ldys} T cells are abundant, transcriptionally distinct, and mutually exclusive in the TIL of human NSCLC samples. Gueguen *et al.* (*53*) found minimal TCR sequence overlap between the *KLF2* and *GZMK* clusters with the *LAYN* cluster, suggesting that, similar to our observations made in the mouse model, human $CD8^+$ T cells enriched for the T_{Ldys} signature inefficiently differentiated to terminally exhausted TIL.

To validate that the T_{Ldys} gene signature could also be detected in other NSCLC datasets, we mapped gene signatures of T_{ex} or T_{Ldys} T cell states onto three additional NSCLC datasets (*54*–*56*). We found that across NSCLC datasets, most of the $CD8^+$ TIL appeared enriched for the T_{Ldys} signature, whereas only a fraction of TIL were enriched for the T_{ex} signature (Fig. 6E). For individual patients, the contribution of the T_{Ldys} and T_{ex} phenotype varied drastically, supporting the notion that a fraction of patients with NSCLC completely lack a population of T cells in the T_{ex} state found in KP flank tumors and are dominated by the T_{Ldys} phenotype found in KP lung tumors (Fig. 6F). In summary, we were able to validate that the T_{Ldys} T cell state is detectable in human NSCLC TIL, and similar to our observation in the mouse model, they have limited differentiation to the T_{ex} state despite signs of T cell activation.

IL-2 and IL-12 therapy prevents T_{Ldys}

Our data suggested that the T_{Ldys} state was induced during T cell priming in the mLN, where transcriptional profiling indicated significantly lower expression of *Il2ra*, *Il12rb*, and *Il12rb2* (Fig. 4B). In addition, pathway analysis had found that IL-2 signaling was significantly enriched in flank TIL compared with lung TIL (Fig. 2F). Given these observations, we determined whether cytokine therapy with IL-2 or IL-12 could prevent T_{Ldys} induction in our model. To deliver IL-2 or IL-12 to tumor-bearing mice, we used fusion proteins of IL-2 or IL-12 to murine serum albumin (MSA) (MSA-IL2 and MSA-IL12, respectively), which lengthens the half-life of IL-2 or IL-12 in vivo and has potent antitumor effects in mouse flank tumor models (*57*, *58*). We transferred 2C T cells to mice bearing KP.SIY lung tumors and, on the same day, administered MSA-IL2 or MSA-IL12. MSA-IL2 treatment slightly increased CD25 and GzmB expression, whereas MSA-IL12 had no effect (Fig. 7B). Combined administration of MSA-IL2 and MSA-IL12 led to a significant increase in both CD25 and GzmB (Fig. 7B). To determine whether differentiation of endogenous T cells to the T_{Ldys} state could be overcome, we treated mice bearing KP.SIY lung tumors with MSA on day 7 after tumor inoculation and analyzed the endogenous SIY-reactive $CD8^+$ T cells in mLN and tumors on day 10 after tumor inoculation. SIY-reactive $CD8^+$ T cells in the mLN down-regulated TCF-1 and up-regulated TIM-3 (Fig. 7C), CD25, GzmB, and 4-1BB, whereas CD49d was unchanged (Fig. 7D). We also found a notable up-regulation of TIM-3, CD25, GzmB, and 4-1BB (Fig. 7, E and F) and a modest down-regulation of CD49d expression (Fig. 7F) in SIY-reactive $CD8^+$ TIL, indicating that IL-2 and IL-12 were sufficient to overcome T_{Ldys} in our model.

On the basis of the significant change in T cell differentiation induced by MSA-IL2 and MSA-IL12, we next assessed whether this therapy could induce control of KP lung tumors. Mice were inoculated with KP parental lung tumors and treated with ICB, MSA-IL2, and MSA-IL12 or the combination on day 7 (Fig. 7G). ICB had no effect on tumor growth (Fig. 7, H and I), whereas MSA-IL2 and MSA-IL12 and the combination of ICB + MSA-IL2 and MSA-IL12 induced marked reductions in lung KP tumors on day 21 (Fig. 7, H and I). In addition, a longitudinal study using micro–computed tomography found that MSA-IL2 and MSA-IL12 treatment even reduced tumor size over time (fig. S7, A and B, and movies S1 to S4).

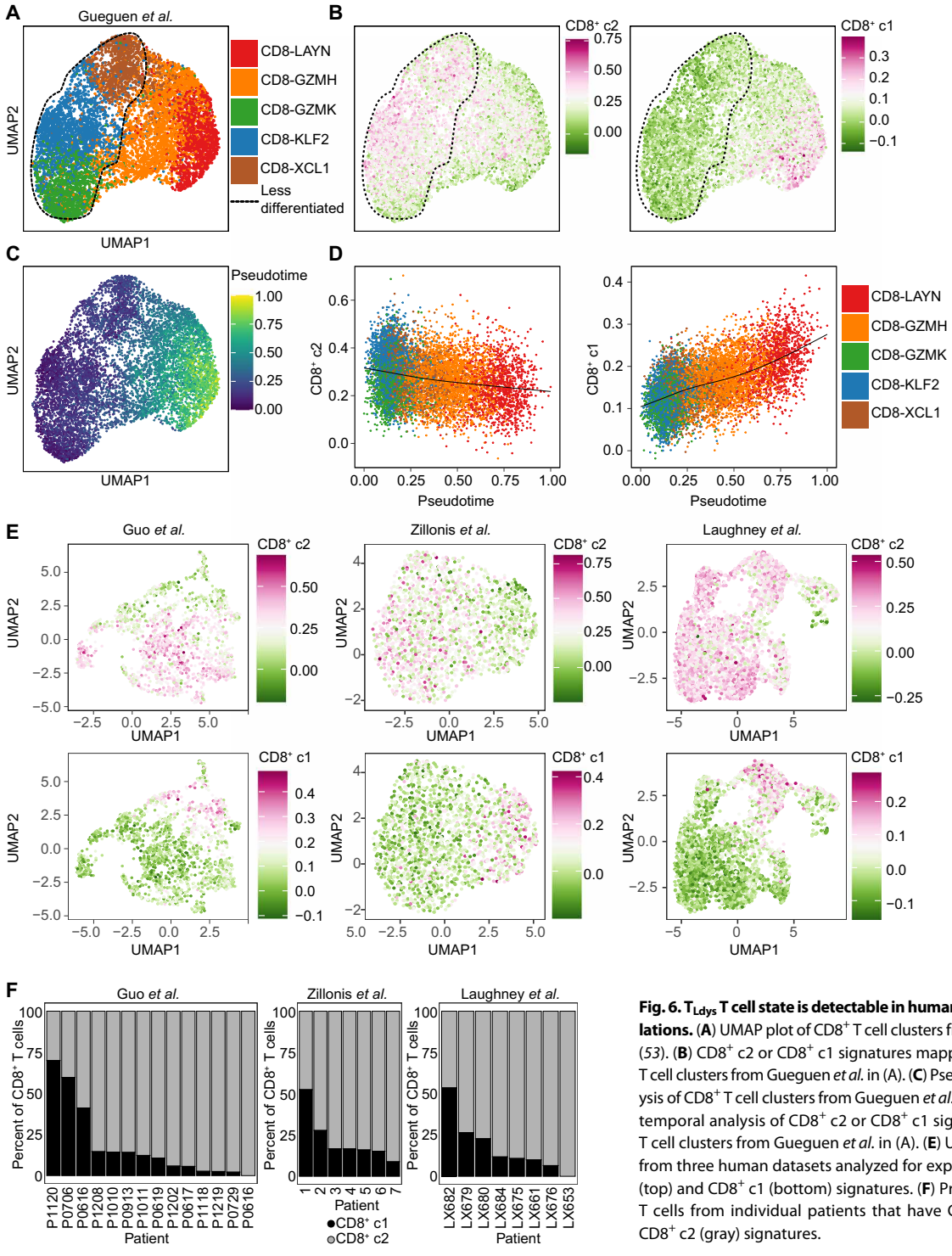

Fig. 6. T_{Ldys} T cell state is detectable in human NSCLC TIL populations. (**A**) UMAP plot of $CD8^+$ T cell clusters from Gueguen *et al.* (*53*). (**B**) $CD8^+$ c2 or $CD8^+$ c1 signatures mapped onto the $CD8^+$ T cell clusters from Gueguen *et al.* in (A). (**C**) Pseudotemporal analysis of $CD8^+$ T cell clusters from Gueguen *et al.* in (A). (**D**) Pseudotemporal analysis of $CD8^+$ c2 or $CD8^+$ c1 signatures and $CD8^+$ T cell clusters from Gueguen *et al.* in (A). (**E**) UMAP feature plots from three human datasets analyzed for expression of $CD8^+$ c2 (top) and $CD8^+$ c1 (bottom) signatures. (**F**) Proportions of $CD8^+$ T cells from individual patients that have $CD8^+$ c1 (black) or $CD8^+$ c2 (gray) signatures.

Consistently, MSA-IL2– and MSA-IL12–treated mice had significantly longer survival (Fig. 7J). Consistent with previous reports (*57*), KP flank tumors also benefitted from MSA-IL2 and MSA-IL12 (fig. S8), suggesting that this therapy also enhances T cell responses in flank TIL. In summary, our data suggest that $CD8^+$ T cells with T_{Ldys} fail to respond to ICB but respond to combined IL-2 and IL-12 treatment in the KP lung tumor model.

DISCUSSION

We identified a state of T cell dysfunction induced during T cell priming in the mLN of KP lung tumor–bearing mice, which we termed T_{Ldys}. T_{Ldys} was characterized by reduced expression of effector and exhaustion molecules on $CD8^+$ T cells and ICB resistance (Fig. 8). T_{Ldys} resembles T cell responses in an ICB-refractory subset of human NSCLCs that have been referred to as nonfunctional.

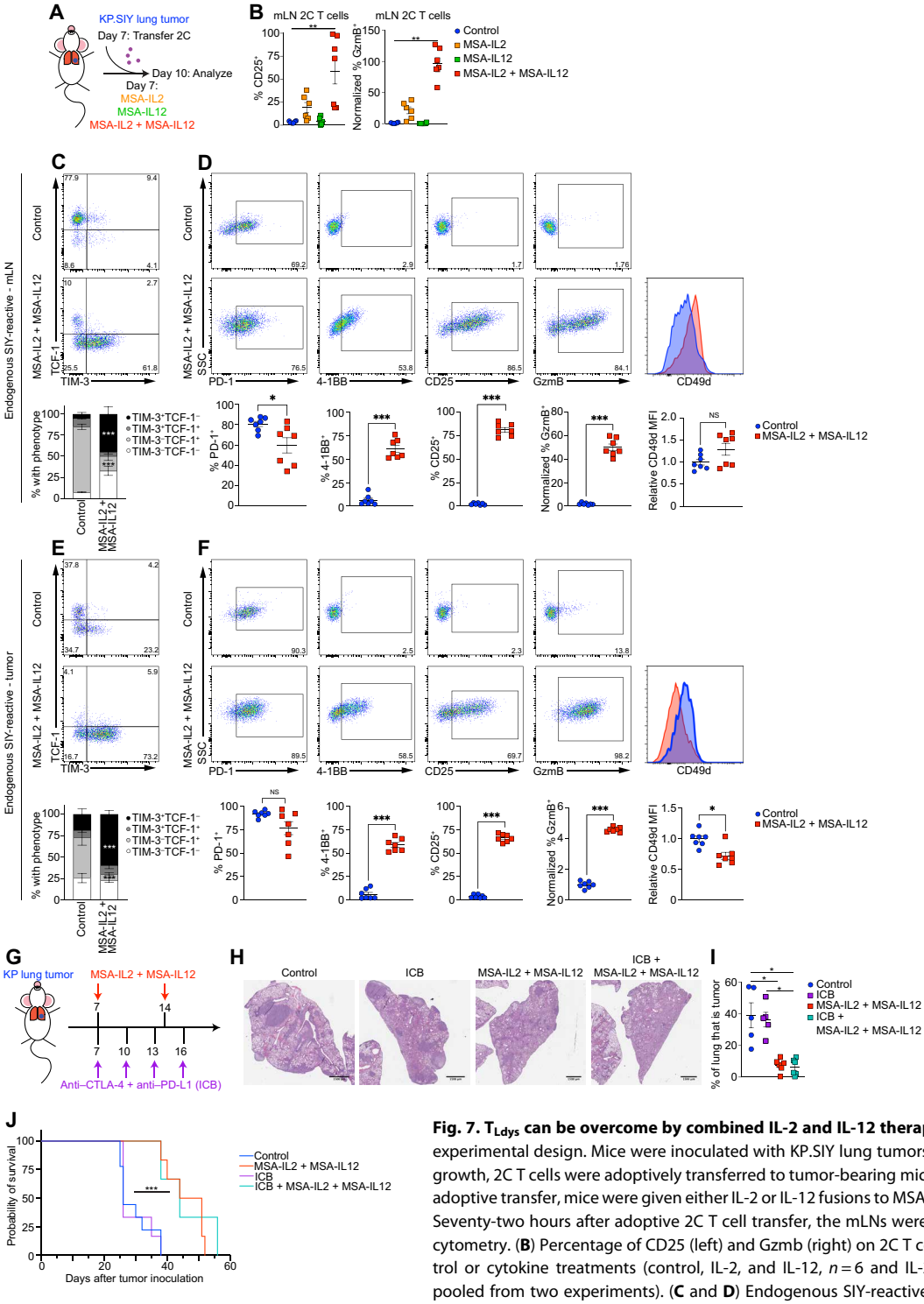

Fig. 7. T_{Ldys} can be overcome by combined IL-2 and IL-12 therapy. (**A**) Schematic of experimental design. Mice were inoculated with KP.SIY lung tumors. On day 7 of tumor growth, 2C T cells were adoptively transferred to tumor-bearing mice. Immediately after adoptive transfer, mice were given either IL-2 or IL-12 fusions to MSA or the combination. Seventy-two hours after adoptive 2C T cell transfer, the mLNs were analyzed with flow cytometry. (**B**) Percentage of CD25 (left) and Gzmb (right) on 2C T cells in mLNs for control or cytokine treatments (control, IL-2, and IL-12, $n = 6$ and IL-2 + IL-12, $n = 7$, data pooled from two experiments). (**C** and **D**) Endogenous SIY-reactive $CD8^+$ T cells in the mLNs were analyzed for (C) TCF-1 and TIM-3 expression or (D) for PD-1, 4-1BB, CD25, GzmB, and CD49d expression. (**E** and **F**) Analysis of endogenous SIY-reactive $CD8^+$ TIL from the same mice as (C) and (D). (E) TCF-1 and TIM-3 expression. (F) PD-1, 4-1BB, CD25, GzmB, and CD49D expression. [(C to F) $n = 7$ each condition, data pooled from two experiments] (**G**) Schematic of experiment combining ICB with MSA-IL2 + MSA-IL12 therapy. Mice were inoculated with KP.SIY lung tumors. Mice received either control treatments, ICB on days 7, 10, 13, and 16, MSA-IL2 + MSA-IL12 on days 7 and 10, or the combination of ICB and MSA-IL2 and MSA-12. (**H** and **I**) Lung tumor burden assessed on day 21 with (H) showing a representative H&E example and (I) showing the quantification of tumor area per lung lobe (control and ICB, $n = 5$ and MSA-IL2 + MSA-IL12 and ICB + MSA-IL2 + MSA-IL12, $n = 6$, data pooled from two experiments). (**J**) Mice were inoculated with lung KP tumors, treated as in (G), and monitored for survival (control, $n = 9$; ICB, $n = 6$; MSA-IL2 + MSA-IL12, $n = 6$; and ICB + MSA-IL2 + MSA-IL12, $n = 3$; data pooled from three experiments). Data are shown as means ± SEM, and statistical analysis was conducted using an MWU test with $^*P < 0.05$, $^{**}P < 0.01$, and $^{***}P < 0.001$ (B to I), or with a Kaplan-Meier analysis (J).

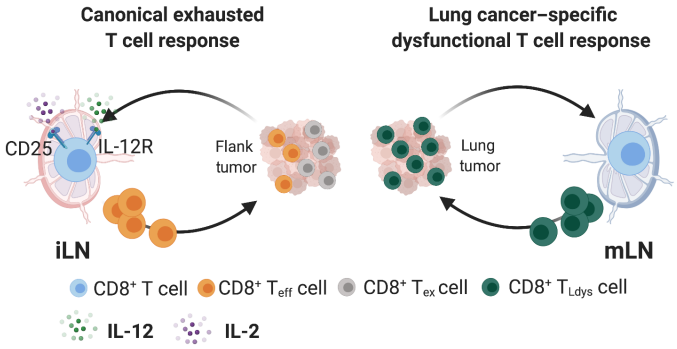

Fig. 8. Schematic summary. (**Left**) In response to flank tumors, tumor-reactive $CD8^+$ T cells primed in the iLN up-regulate CD25 and IL-12R, express effector molecules, show signs of conventional exhaustion, and respond to CBT. (**Right**) In response to lung tumors, however, tumor-reactive $CD8^+$ T cells primed in the mLN activate a lung-specific dysfunctional program (T_{Ldys}), do not up-regulate CD25 and IL-12R, fail to gain effector molecule expression, and do not acquire a conventional T_{ex} phenotype. $CD8^+$ TLdys cells do not respond to CBT. This suggests that differentiation of $CD8^+$ T cells into dysfunctional states other than conventional T_{ex} drives CBT resistance in a subset of T cell–infiltrated NSCLCs. T_{eff}, effector T cell. Created with Biorender.com.

In this subset of patients, tumors are infiltrated by T cells, but these T cells fail to up-regulate effector molecules and PD-L1 in response to ICB (*3*). Therefore, our observations on the induction and characteristics of the T_{Ldys} T cell state may allow for the rational development of new treatment strategies for T cell–infiltrated but ICB-refractory NSCLC.

T cell infiltration into tumors is predictive for ICB response, but the quality of T cells is critical (*40*). We provide evidence that not all tumor-reactive T cells are functionally interchangeable and that not all tumor-specific $CD8^+$ T cells will react to ICB. T cells with T_{Ldys}, induced in response to orthotopic lung cancer, failed to produce IFN-γ, a feature of antitumor immune responses that mediate PD-L1 up-regulation, a biomarker in NCSLC. ICB failed to expand TIL T_{Ldys} and did not affect the phenotype or function of lung tumor–reactive T cells. Furthermore, T cells with T_{Ldys} had low GzmB and poor cytotoxicity in vivo. Thus, T_{Ldys} closely resembles the nonfunctional T cell responses described in an ICB-refractory NSCLC patient population (*3*, *59*–*62*). In contrast, flank TIL gained effector function and responded to ICB with T cell expansion and tumor control, suggesting that T_{Ldys} was specific to orthotopic lung tumors.

We determined that T cell fate decisions leading to T_{ex} or T_{Ldys} occurred during priming in the TdLN. Transcriptional differences occurred within 72 hours after T cell activation. T cells primed in the mLN never gained robust CD25 expression, whereas priming in the iLN resulted in CD25 up-regulation. $CD8^+$ T cells that express high levels of CD25 differentiate into effector T cells (*38*, *39*), suggesting that CD25 expression is required for differentiation into effector and exhausted T cell states. Consistently, T cells primed in the mLN had low GzmB, a phenotype that was preserved in lung TIL. These data suggested that T cell fate decisions are made early during T cell priming, depend on the local cytokine milieu, and can predetermine the quality of the resulting TIL.

T cell activation is affected by antigen drainage to the TdLN and the functional capacity of APC. We found comparable antigen load and stimulatory capacity of DC between lung and flank tumors. T_{Ldys} was also observed with intratracheal administration of tumor cells, a condition used to control for potential systemic dissemination of tumor cells or different tumor loads induced between intravenous and subcutaneous settings. However, it remains a possibility that greater immunogenic cell death is induced in flank tumors, leading to a more inflammatory environment and thus effective $CD8^+$ T cell activation. Alternatively, the lung could be a tolerogenic environment (*63*), requiring a greater degree of immunogenic cell death for innate immune activation. It should be noted, however, that only inoculation of lung cancers KP and LL/2 into the lung induced T_{Ldys}, whereas inoculation of B16 melanoma cells resulted in T_{ex}, suggesting that only orthotopic lung tumors may induce T_{Ldys}. Additional tumor cell lines and modes of cancer induction will be needed to fully elucidate the details resulting in T_{ex} or T_{Ldys} induction and whether induction of T_{Ldys} is restricted to the mLN. Our analyses indicate the presence of both phenotypes in flank TIL, suggesting that T cell differentiation may be complex.

Adoptive transfer studies suggested that T_{Ldys} persisted after T cell activation. Neither homeostatic proliferation in $RAG2^{-/-}$ mice nor ICB treatment induced effector function, supporting that epigenetic imprinting might mediate T_{Ldys} (*64*, *65*). We found increased *Tox* levels in T cells primed in the mLN. Tox is an epigenetic modifier, previously found to be a critical factor for not only epigenetic remodeling of the chromatin during induction and maintenance of T_{ex} but also long-lived memory T cell responses (*42*, *66*). In addition, Tox expression was found in stem-like memory $CD8^+$ T cells induced after intravenous nanoparticle vaccine administration (*67*). Therefore, we speculate that Tox up-regulation during induction of the T_{Ldys} suggests a context-specific effect of Tox. Further assessment of the epigenetic state of T_{Ldys} and T_{ex} will be needed to fully elucidate whether Tox or additional epigenetic modifiers are important for the induction of T_{Ldys} and how the epigenetic state of T_{Ldys} compares with other T cell states.

Consistent with decreased expression of CD25 and GzmB after priming in the mLN, we found decreased differentiation of $CD8^+$ T cells into $TIM\text{-}3^+$ effector cells. TCF-1 and TIM-3 define precursor- and terminally exhausted $CD8^+$ T cells, respectively, in chronic LCMV and melanoma models (*36*, *37*, *40*, *47*, *51*). Expression of $TCF1^+$ in SIY-reactive T cells in the mLN together with elevated levels of *Tox*, *Bach2*, and *Bcl6* suggested a relation to precursor-exhausted $CD8^+$ T cells (*47*). However, adoptive transfer studies of 2C T cells primed in mLN clearly demonstrated that T cells with T_{Ldys} failed to differentiate into effector or exhausted T cells. Direct comparison of $CD8^+$ TIL from KP lung tumors to transcriptional signatures of precursor-exhausted $CD8^+$ T cells suggested that T cells with T_{Ldys} do not transcriptionally resemble precursor-exhausted $CD8^+$ T cells. These data suggest that T_{Ldys} is induced early and does not give rise to conventionally exhausted T cells.

Integration of our findings with clinical datasets suggested that a fraction of T cell–infiltrated patients lacked exhausted T cells and were dominated by T_{Ldys} T cells. A recent publication described five $CD8^+$ TIL populations in NSCLC: blood-derived CD8-KLF2 and CD8-GZMK precursors, tumor-infiltrating CD8-XCL1 precursors, a transitory CD8-GZMH population, and terminally exhausted CD8-LAYN T cells (*53*). Mapping the T_{Ldys} signature onto this dataset suggested a close association of T cells with T_{Ldys} with KLF2 and GZMK precursor clusters, whereas the exhaustion signature derived from $CD8^+$ c1 T cells mapped to the exhausted LAYN cluster. Gueguen *et al.* (*53*) found limited differentiation of KLF2 and GZMK precursor populations to exhausted LAYN T cells, consistent with our data that T cells with T_{Ldys} failed to acquire effector and exhaustion molecules.

Multiple studies found that exhausted $CD8^+$ T cells correlate with good responses to ICB in patients with NSCLC (*60*–*62*), and the presence of a T cell–derived IFN-γ signature and PD-L1 up-regulation is predictive for ICB response in NSCLC. This is supported by our studies in which T_{Ldys} T cells failed to respond to ICB or make IFN-γ; therefore we propose that the patient populations dominated by T_{Ldys} T cells may represent patients that would be ICB refractory. However, this requires clinical validation. We also showed that IL-2/IL-12 cytokine treatment could mediate differentiation of T_{Ldys} T cells into highly potent effector T cells. This observation demonstrates that whereas T_{Ldys} T cells fail to spontaneously differentiate into effector T cells, cytokine therapy could facilitate this differentiation. Further studies will be required to determine the phenotype of T cells responding to IL-2/IL-12 therapy in flank tumors because about 50% of flank TIL were of T_{Ldys} T cell state. How natural cytokine signals might affect the spontaneous differentiation into T_{ex} and T_{Ldys} state will also require additional interrogations. However, immunosuppressive populations such as regulatory T cells or tumor-associated macrophages might affect T cell differentiation by cytokine production or consumption (*68*, *69*).

Whereas Gueguen *et al.* (*53*) found limited evidence for transition of T cell clonotypes from the *KLF2* or *GZMK* clusters to the *LAYN* cluster, our TCR clonotype analyses identified shared clonotypes between T_{ex} and T_{Ldys}. Furthermore, we were able to demonstrate the induction of T_{Ldys} and exhausted T cell phenotypes among endogenous SIY-reactive T cells in KP.SIY tumors and in TCR-transgenic T cells. In addition, only subtle differences between the $CD8^+$ TIL responses against KP and KP.SIY tumors were found. Together, these observations provide strong support that decisions between T_{ex} and T_{Ldys} are independent of TCR usage or affinity. Whether TCR signal strength affects T cell states in the TME requires further investigation. In summary, analyses of both clinical samples and our mechanistic studies agree that T cell priming in LN is involved in inducing different T cell states and highlights the importance of further understanding the determinants of early T cell fate decisions.

To determine whether the T_{Ldys} phenotype could be therapeutically manipulated, we assessed whether cytokine therapy might be effective when administered during priming. Combined treatment with IL-2 and IL-12 induced differentiation of T_{Ldys} to an effector T cell state. This raises questions about IL-2 and IL-12 signals during priming. IL-2 availability can be significantly affected by immunosuppressive populations such as regulatory T cells (*70*, *71*). Regulatory T cells, in turn, are frequently localized to tissue-draining LN based on tissue-specific antigen expression patterns (*72*, *73*). Lung-specific regulatory T cells may therefore affect effector T cell activation in the mLN. IL-12 is produced by myeloid cells (*74*), but the exact cellular source of IL-12 is still unclear. It is conceivable that IL-12 is induced once $CD8^+$ T cells gain the ability to produce IFN-γ (*75*). IL-12 has also been shown to induce down-regulation of *Klf2* and *S1pr1* expression in T cells (*76*). Down-regulation of *KLF2* and *S1PR1* is a common feature of $CD8^+$ T cells that express high levels of PD-1, LAG-3, TIM-3, and 4-1BB both in human TIL (*59*–*62*) and TIL isolated from KP flank tumors. This together with the requirement of IL-2 might suggest that IL-2 and IL-12 signaling sensitizes T cells during priming for the optimal acquisition of effector function. Thus, IL-2– and IL-12–based immunotherapies may help differentiate TIL toward an ICB-responsive state. In a recent study, new derivatives of IL-12 were generated to reduce natural killer cell–mediated toxicity but retain the ability of IL-12 to induce T cell effector function, primarily IFN-γ and GzmB (*77*). This preclinical work, together with our observations, points to a potential use for cytokine therapy in patients with nonfunctional T cell responses who fail to respond to current treatments.

One shortcoming of our studies was that we could not separate lung tumors and normal lung tissue, and therefore, we cannot fully exclude that T cells from healthy lung affect our analysis; however, our IF experiments suggest that TIL were strongly enriched in the TME. Another shortcoming was that our study is based on a limited number of transplantable cell lines and tumor inoculation methods. In addition, there were insufficiently available human NSCLC data to determine whether the gene signature associated with $CD8^+$ c2 is predictive of ICB resistance. Future longitudinal human studies comparing ICB outcome with pretreatment $CD8^+$ TIL scRNA-seq will be required to address this question.

Together, our data suggest that responsiveness to ICB in NSCLC can be predetermined during T cell priming in the mLN. If T cells enter T_{Ldys}, a T cell response lacking cytotoxic effector functions becomes established in tumors. It is conceivable that this early decision point precludes T cells with T_{Ldys} from reinvigoration by ICB. This study provides mechanistic insight into the induction of ICB-refractory T cell responses and provides rationale for potential strategies to increase effector $CD8^+$ T cell differentiation in NSCLC, potentially benefiting ICB-refractory patients with nonfunctional immune responses, improving outcomes for patients with NSCLC.

MATERIALS AND METHODS

A full description of the methods can be found in Supplementary Methods.

Study design

The purpose of this study was to determine how differences in T cell activation between lung and flank KP tumors led to ICB resistance in KP lung tumors. We characterized T cell differentiation in these two tumor settings and defined how this contributed to ICB resistance. We used transplantable syngeneic tumor mouse models and publicly available human datasets. Mice were randomized into study groups after tumor inoculation and before treatments. All experiments were performed at least twice independently with at least three mice per group. All data were included unless there were technical issues with experimental setup or data collection. Outliers were not removed. All tumor outgrowth studies were planned to end on day 21 after tumor injection. Early termination occurred if tumors grew past the allowed size or if mice were flagged by veterinarians for tumor ulceration, changes in body condition, or other health reasons that required euthanasia before day 21. Other tumor analysis time points were days 7 and 14 after tumor injection or 3 days after adoptive transfer of transgenic T cells.

Mice

All mice were housed and bred under specific pathogen–free conditions at the Koch Institute animal facility. All experimental animal procedures were approved by the Committee on Animal Care at the Massachusetts Institute of Technology (MIT).

Generation of expression vectors

The pLV-EF1α-IRES-puro vector (Addgene no. 85132) was used in conjunction with the cerulean-SIY insert generated using the

Cerulean-N1 template (Addgene no. 54742) or the ZsGreen insert zsGreen_minOVA (a gift from M. Krummel).

Tumor cell lines and tumor outgrowth studies

KP, LL/2, KP.SIY, and B16.SIY were cultured under standard conditions. Tumor cells (2.5×10^5) were injected. Subcutaneous tumor area measurements were collected two to three times a week, whereas lung tumor areas of hematoxylin and eosin (H&E) sections were measured using QuPath software.

Immunohistochemistry

Flank tumors and tumor-bearing lungs were fixed in 10% formalin. Fixed tissues were processed, paraffin-embedded, sectioned, and stained by the Hope Babette Tang Histology Facility at the Koch Institute at MIT. For anti-CD8 staining, a 1:200 dilution of anti-CD8 (clone 4SM16, eBioscience 14-0195-82) was used.

Immunofluorescence

Tumors were processed as previously described (*78*). Tissues were stained with antibodies (see the Supplementary Materials) and washed with phosphate-buffered saline (PBS), and nuclei were counterstained with propidium iodide. Tissue sections were imaged using the TissueFAXS whole-slide scanning system (TissueGnostics, USA) using a Zeiss 20x Plan-Neofluar air, 0.5 numerical aperture and analyzed using the TissueQuest image analysis software (TissueGnostics, USA). Images were processed with the image processing package FIJI (*79*).

Tumor dissociation

Spleens and LNs were dissected from mice and physically dissociated. Tumors were dissociated using the gentleMACS Octo Dissociator (Miltenyi).

Flow cytometry and cell sorting

All analyses excluded circulating $CD45^+$ cells using intravenous injection of a PE-CF594–labeled anti-CD45 antibody before euthanasia, which allowed circulating cells to be excluded from analyses. Cells were resuspended in antibody-containing staining buffer plus eBioscience Fixable Viability Dye eFluor 780 or eFluor 506 to distinguish live and dead cells and with anti-CD16/CD32 to prevent nonspecific antibody binding. Cell surface proteins were stained for 20 min on ice with fluorophore-conjugated antibodies at a 1:200 dilution. Cells were washed and resuspended in fixation/permeabilization buffer followed by staining with antibodies against intracellular targets. To obtain absolute counts of cells, Precision Count Beads (BioLegend) were added. Flow cytometry sample acquisition was performed on an LSRFortessa cytometer (BD Biosciences), and the collected data were analyzed using FlowJo v10.5.3 software (TreeStar). For cell sorting, the surface staining was performed as described above under sterile conditions, and cells were acquired and sorted into TRIzol or buffer using a FACSAria III sorter (BD Biosciences). For TIL analysis, cells were pregated on live, $CD45^+$, $CD45\text{-}IV^-$, $TCR\beta^+$, single cells, $CD4^-$, and $CD8^+$. See the Supplementary Materials for all antibodies. See fig. S9 for example gating strategy of $CD8^+$ and SIY-reactive $CD8^+$ cells.

Seq-Well sequencing and analysis

Single-cell suspensions were prepared as described above. Mice received anti–CD45-PE antibody retro-orbitally 3 min before euthanasia, followed by bead-mediated depletion of antibody-labeled circulating cells. SIY pentamer–reactive $CD8^+$ T cells were isolated using FACS. Cells were then processed using the Seq-Well platform with second strand chemistry, as previously described (*16*, *33*). Libraries were barcoded and amplified using the Nextera XT kit (Illumina) and were sequenced on a NovaSeq 6000 or a NextSeq 550 (Illumina).

Single-cell data processing and visualization

Raw read processing of scRNA-seq reads was performed as previously described (*80*). Principal components analysis was performed. The number of principal components used for visualization was determined by examination of the elbow plot, and two-dimensional embeddings were generated using UMAP. Clusters were determined using Louvain clustering, as implemented in the FindClusters function in Seurat, and clusters that contained T cells were selected for further analysis. These cells were reprocessed with the same processing and clustering steps described above. Differential gene expression was performed for each cluster, and clusters corresponding to similar phenotypes were merged.

Pathway enrichment analysis

Gene sets representing relevant pathways were obtained from MSigDB (*81*, *82*). A score for the expression of genes in each pathway was calculated for each cell using the AddModuleScore function in Seurat (*83*). Pathways in the hallmarks gene collection were used to analyze $CD8^+$ T cells and KP.zsGreen tumor cells.

Paired single-cell TCR sequencing

Paired TCR sequencing and read alignment was performed as previously described (*84*). Processing of reads was performed using the Immcantation software suite (*85*, *86*). GLIPH2 analysis was performed as described previously (*34*) using the provided data from mouse $CD8^+$ T cells as a reference. For the analysis of global motifs, substitutions between any pair of amino acids were permitted. GLIPH specificity groups that were subsets of other specificity groups were not analyzed further.

Integrated analysis of KP parental and KP.SIY single-cell data

Single-cell sequencing data from KP parental and KP.SIY TIL were integrated using Seurat v3 (*87*). Genes that were detected in less than 3% of cells in either the KP TIL or KP.SIY TIL were excluded. Default parameter values and the top 30 canonical correlation analysis (CCA) components were used to find transfer anchors between datasets and generate an integrated matrix.

Adoptive TIL transfer

Flank and lung tumors were dissociated and prepared for FACS as described above. TIL were identified as Live, $CD45^+$, noncirculating $Thy1^+$ cells. Recipient $RAG2^{-/-}$ mice received equal numbers (20,000) of either lung or flank TIL intravenously. TIL were allowed more than 12 weeks to reconstitute $RAG2^{-/-}$ mice, after which the reconstituted mice were inoculated with flank tumors.

Concomitant immunity assay

Mice were injected with KP tumors subcutaneously or intravenously as outlined above. Seven days after tumor injection, mice were injected with a second KP tumor on the contralateral flank or intravenously.

CD8 antibody depletion

Mice were injected with 200 μg of anti-CD8 antibody (clone 53-6.7 Bio X Cell) weekly for the duration of the experiment, beginning 48 hours before tumor inoculation.

IFN-γ–ELISpot

Splenocytes (1×10^6) were plated on coated and washed ELISpot plates and stimulated with 160 nM SIY peptide or a mixture of phorbol 12-myristate 13-acetate (100 ng/ml; Sigma-Aldrich) and ionomycin (1 μg/ml; Sigma-Aldrich) as a positive control or medium only as negative control. Plates were developed the next day using the BD Biosciences mouse IFN-γ–ELISpot kit, following the manufacturer's protocol.

2C T cell adoptive transfer

T cells were isolated from 2C RAG2$^{-/-}$CD45.1$^+$ mice (spleen and LN) and labeled with CFSE or CellTrace Violet (Life Technologies). T cells (10^6) were transferred to mice bearing KP.SIY tumor 7 days after tumor inoculation and isolated 72 hours later. For CFSE analysis, the percent proliferated was calculated as the percentage of cells that had undergone one or more rounds of division based on CFSE staining intensity using an unstimulated, CFSE-labeled sample as an undivided reference control. For transfers into secondary recipients, 2C T cells were transferred into primary recipients as described above, isolated from mLN or iLN, and enriched using the Miltenyi CD8$^+$ T cell isolation kit before CD45.1$^+$ 2C T cells were sorted using FACS. Sorted cells were transferred intravenously into secondary recipient RAG2$^{-/-}$ mice bearing day 7 flank KP.SIY tumors. Secondary recipients were analyzed 5 days after adoptive transfer.

DC analysis and ex vivo coculture assay

LN processing procedure was adapted from Ruhland *et al.* (*45*), and CD19$^+$ and CD3$^+$ cells were depleted using magnetic beads before flow analysis or sort of DC. For ex vivo cocultures, OT-I T cells were isolated and CFSE-labeled as described above. CD8$^+$ OT-I cells (5×10^4) and FACS-sorted ZsGreen$^+$ DCs (5×10^3) were cocultured and analyzed by flow cytometry at 72 hours.

Smart-seq bulk RNA-seq and analysis

2C T cells were adoptively transferred to tumor-bearing mice as described above. Seventy-two hours after transfer, TdLN cells were isolated and prepared for FACS. 2C T cells were FACS-sorted directly into TRIzol reagent and RNA-extracted. RNA library preparation and sequencing were performed at the KI Genomics Core / MIT BioMicro Center. Sequencing was performed using the HiSeq 2000 sequencing system (Illumina). Sequence alignment and .bam file generation were performed by the KI Genomics Core / MIT BioMicro Center. The resulting .bam files were sorted using Samtools. Differential gene expression analysis was performed on the sorted .bam files with Cufflinks.

Analysis of data from Chen *et al.*

Data from the scRNA-seq of P14 cells published by Chen *et al.* (*36*) were downloaded from the Gene Expression Omnibus (GEO) database under accession number GSE131535. The data were processed using the processing pipeline described above, and clusters were determined using the FindClusters function in Seurat. Gene signature scores were calculated using the AddModuleScore function in Seurat.

Cytokine and detection

Single-cell suspensions were isolated from tumors as described above. Round-bottom 96-well plates were coated overnight in PBS with anti-CD3 (0.2 μg/ml; clone 145-2C11, BD Biosciences), and anti-CD28 (0.5 μg/ml; clone 37.51, BD Biosciences). Cells were plated in coated round-bottom 96-well plates for 4 hours in the presence of BrefeldinA (BioLegend). After 4 hours, the cells were stained for extracellular and intracellular antigens.

In vivo cytotoxicity assay

The protocol was adapted from Kim *et al.* (*52*). Wild-type splenocytes were ammonium-chloride-potassium–lysed and pulsed for 1 hour at 37°C with 0.2 μM SIY peptide. SIY-pulsed splenocytes were then labeled with 0.5 μM CFSE, whereas control, unpulsed splenocytes were labeled with 5 μM CFSE for 10 min at 37°C. After CFSE labeling, SIY-pulsed and control splenocytes were mixed at a 1:1 ratio, and 10×10^6 of each were intravenously injected into mice bearing KP.SIY lung or flank tumors on day 7 of tumor growth or into naïve control mice. Four hours after injection of CFSE-labeled splenocytes, spleens from tumor-bearing mice were isolated, single-cell splenocyte suspensions were generated by physical dissociation, and splenocytes were stained with a live/dead discriminator dye and analyzed for CFSE$^+$ populations by flow cytometry.

Analysis of human NSCLC datasets

Human NSCLC single-cell datasets were downloaded from the GEO database, under accession numbers GSE99254 (*54*), GSE127465 (*56*), GSE123902 (*55*), and GSE162500 (*53*). Data from Gueguen *et al.* (*53*) were processed using integration in Seurat 3, as described by Stuart *et al.* (*87*). Gene signature scores were computed using the AddModuleScore function in Seurat. Pseudotemporal ordering using diffusion pseudotime was performed using sc.tl.dpt function in SCANPY (*88*, *89*). Data from Guo *et al.* (*54*), Zillonis *et al.* (*56*), and Laughney *et al.* (*55*) were processed using the processing pipeline described above to identify clusters corresponding to CD8$^+$ T cells. Gene signature scores were computed using the AddModuleScore function in Seurat. Clusters were identified using the FindClusters function in Seurat and were classified as CD8$^+$ c1 or CD8$^+$ c2 according to their expression of the corresponding gene signatures.

ICB treatment

Mice were injected intraperitoneally with anti–CTLA-4 (clone UC10-4F10-11) and anti–PD-L1 (clone 10F.9G2) antibodies on days 7, 10, 13, and 16 after tumor inoculation. Each mouse received 100 μg of each antibody per treatment.

MSA-IL2 and MSA-IL12 generation

MSA-cytokine fusions were generated as previously described (*57*, *58*). Human embryonic kidney (HEK) 293 cells were transfected with plasmid DNA using polyethylenimine in OptiPro serum-free medium (Thermo Fisher Scientific). His-tagged proteins were isolated from HEK293 supernatant using TALON Metal Affinity Resin (Takara Bio Inc.). Cytokine fusion proteins were then further purified by size exclusion chromatography using a HiLoad 16/600 Superdex 200 pg column on an ÄKTA fast protein liquid chromatography system (GE Healthcare). All proteins were stored at 4°C, but before therapeutic injection, cytokine fusion proteins were warmed to room temperature.

MSA treatment

Each mouse was injected retro-orbitally with MSA-IL2 (5.94×10^{-10} mol per mouse) and/or MSA-IL12 (1.42×10^{-11} mol per mouse) per treatment. For experiments phenotyping 2C T cells or endogenous SIY-reactive $CD8^+$ T cells, mice received one dose of MSA-cytokine fusions on day 7 after tumor inoculation and were analyzed on day 10 after tumor inoculation. For therapeutic experiments, mice were dosed with MSA-IL2 and/or MSA-IL12 on days 7 and 14 after tumor inoculation and analyzed on day 21 after tumor inoculation and monitored for survival after treatment.

Micro–computed tomography

A Bruker Skyscan 1276 was used to acquire a series of images with a rotation step of 0.65° over a 360° rotation. Images were acquired with x-ray tube settings of 100 kV, 200 μA, and an exposure time of 90 ms with a 0.5-mm aluminum beam filter. A 4 × 4 detector binning was used for an isotropic resolution of 40.16 μm. Anesthesia was induced at 3% isoflurane and maintained at 2.0 to 2.5% during imaging, which lasted 76 s. Image reconstruction was performed using the Bruker NRecon software.

Statistical analysis

Statistical analyses were performed using GraphPad Prism (GraphPad) and R. All data are shown as means ± SEM. For flow cytometry, immunohistochemistry, and tumor outgrowth studies, statistical analyses were performed with Mann-Whitney *U* (MWU) test for comparisons of two groups or two-way analysis of variance (ANOVA) for multiple comparisons over time, with $^*P < 0.05$; $^{**}P < 0.01$; $^{***}P < 0.001$; and $^{****}P < 0.0001$. For differential gene expression between T cell clusters, *P* values were calculated using a two-sided Wilcoxon rank-sum test and were corrected with Bonferroni correction. For comparison of gene modules with previously published T cell states, false discovery rate *q* values were calculated using a one-tailed hypergeometric test and were corrected with Bonferroni correction. For pathway analysis, *P* values were calculated using a two-tailed Wilcoxon rank-sum test and were corrected with Bonferroni correction.

SUPPLEMENTARY MATERIALS

www.science.org/doi/10.1126/sciimmunol.abi8800
Methods
Figs. S1 to S10
Tables S1 to S8
Movies S1 to S4

View/request a protocol for this paper from *Bio-protocol*.

REFERENCES AND NOTES

1. S. L. Topalian, F. S. Hodi, J. R. Brahmer, S. N. Gettinger, D. C. Smith, D. F. McDermott, J. D. Powderly, R. D. Carvajal, J. A. Sosman, M. B. Atkins, P. D. Leming, D. R. Spigel, S. J. Antonia, L. Horn, C. G. Drake, D. M. Pardoll, L. Chen, W. H. Sharfman, R. A. Anders, J. M. Taube, T. L. McMiller, H. Xu, A. J. Korman, M. Jure-Kunkel, S. Agrawal, D. McDonald, G. D. Kollia, A. Gupta, J. M. Wigginton, M. Sznol, Safety, activity, and immune correlates of anti–PD-1 antibody in cancer. *N. Engl. J. Med.* **366**, 2443–2454 (2012).
2. H. Rafei, E. El-Bahesh, A. Finianos, S. Nassereddine, I. Tabbara, Immune-based therapies for non-small cell lung cancer. *Anticancer Res* **37**, 377–387 (2017).
3. R. S. Herbst, J. C. Soria, M. Kowanetz, G. D. Fine, O. Hamid, M. S. Gordon, J. A. Sosman, D. F. McDermott, J. D. Powderly, S. N. Gettinger, H. E. Kohrt, L. Horn, D. P. Lawrence, S. Rost, M. Leabman, Y. Xiao, A. Mokatrin, H. Koeppen, P. S. Hegde, I. Mellman, D. S. Chen, F. S. Hodi, Predictive correlates of response to the anti–PD-L1 antibody MPDL3280A in cancer patients. *Nature* **515**, 563–567 (2014).
4. L. Fehrenbacher, A. Spira, M. Ballinger, M. Kowanetz, J. Vansteenkiste, J. Mazieres, K. Park, D. Smith, A. Artal-Cortes, C. Lewanski, F. Braiteh, D. Waterkamp, P. He, W. Zou, D. S. Chen, J. Yi, A. Sandler, A. Rittmeyer; POPLAR Study Group, Atezolizumab versus docetaxel for patients with previously treated non-small-cell lung cancer (POPLAR): A multicentre, open-label, phase 2 randomised controlled trial. *Lancet* **387**, 1837–1846 (2016).
5. J. Larkin, V. Chiarion-Sileni, R. Gonzalez, J. J. Grob, P. Rutkowski, C. D. Lao, C. L. Cowey, D. Schadendorf, J. Wagstaff, R. Dummer, P. F. Ferrucci, M. Smylie, D. Hogg, A. Hill, I. Marquez-Rodas, J. Haanen, M. Guidoboni, M. Maio, P. Schoffski, M. S. Carlino, C. Lebbe, G. McArthur, P. A. Ascierto, G. A. Daniels, G. V. Long, L. Bastholt, J. I. Rizzo, A. Balogh, A. Moshyk, F. S. Hodi, J. D. Wolchok, Five-year survival with combined nivolumab and ipilimumab in advanced melanoma. *N. Engl. J. Med.* **381**, 1535–1546 (2019).
6. P. C. Tumeh, C. L. Harview, J. H. Yearley, I. P. Shintaku, E. J. Taylor, L. Robert, B. Chmielowski, M. Spasic, G. Henry, V. Ciobanu, A. N. West, M. Carmona, C. Kivork, E. Seja, G. Cherry, A. J. Gutierrez, T. R. Grogan, C. Mateus, G. Tomasic, J. A. Glaspy, R. O. Emerson, H. Robins, R. H. Pierce, D. A. Elashoff, C. Robert, A. Ribas, PD-1 blockade induces responses by inhibiting adaptive immune resistance. *Nature* **515**, 568–571 (2014).
7. W. H. Fridman, L. Zitvogel, C. Sautès-Fridman, G. Kroemer, The immune contexture in cancer prognosis and treatment. *Nat. Rev. Clin. Oncol.* **14**, 717–734 (2017).
8. R. Cristescu, R. Mogg, M. Ayers, A. Albright, E. Murphy, J. Yearley, X. Sher, X. Q. Liu, H. Lu, M. Nebozhyn, C. Zhang, J. K. Lunceford, A. Joe, J. Cheng, A. L. Webber, N. Ibrahim, E. R. Plimack, P. A. Ott, T. Y. Seiwert, A. Ribas, T. K. McClanahan, J. E. Tomassini, A. Loboda, D. Kaufman, Pan-tumor genomic biomarkers for PD-1 checkpoint blockade-based immunotherapy. *Science* **362**, eaar3593 (2018).
9. D. B. Doroshow, M. F. Sanmamed, K. Hastings, K. Politi, D. L. Rimm, L. Chen, I. Melero, K. A. Schalper, R. S. Herbst, Immunotherapy in non-small cell lung cancer: Facts and hopes. *Clin. Cancer Res.* **25**, 4592–4602 (2019).
10. J. R. Brahmer, R. Govindan, R. A. Anders, S. J. Antonia, S. Sagorsky, M. J. Davies, S. M. Dubinett, A. Ferris, L. Gandhi, E. B. Garon, M. D. Hellmann, F. R. Hirsch, S. Malik, J. W. Neal, V. A. Papadimitrakopoulou, D. L. Rimm, L. H. Schwartz, B. Sepesi, B. Y. Yeap, N. A. Rizvi, R. S. Herbst, The Society for Immunotherapy of Cancer consensus statement on immunotherapy for the treatment of non-small cell lung cancer (NSCLC). *J. Immunother. Cancer* **6**, 75 (2018).
11. F. Skoulidis, L. A. Byers, L. Diao, V. A. Papadimitrakopoulou, P. Tong, J. Izzo, C. Behrens, H. Kadara, E. R. Parra, J. R. Canales, J. Zhang, U. Giri, J. Gudikote, M. A. Cortez, C. Yang, Y. Fan, M. Peyton, L. Girard, K. R. Coombes, C. Toniatti, T. P. Heffernan, M. Choi, G. M. Frampton, V. Miller, J. N. Weinstein, R. S. Herbst, K. K. Wong, J. Zhang, P. Sharma, G. B. Mills, W. K. Hong, J. D. Minna, J. P. Allison, A. Futreal, J. Wang, I. I. Wistuba, J. V. Heymach, Co-occurring genomic alterations define major subsets of KRAS-mutant lung adenocarcinoma with distinct biology, immune profiles, and therapeutic vulnerabilities. *Cancer Discov.* **5**, 860–877 (2015).
12. F. Skoulidis, M. E. Goldberg, D. M. Greenawalt, M. D. Hellmann, M. M. Awad, J. F. Gainor, A. B. Schrock, R. J. Hartmaier, S. E. Trabucco, L. Gay, S. M. Ali, J. A. Elvin, G. Singal, J. S. Ross, D. Fabrizio, P. M. Szabo, H. Chang, A. Sasson, S. Srinivasan, S. Kirov, J. Szustakowski, P. Vitazka, R. Edwards, J. A. Bufill, N. Sharma, S. I. Ou, N. Peled, D. R. Spigel, H. Rizvi, E. J. Aguilar, B. W. Carter, J. Erasmus, D. F. Halpenny, A. J. Plodkowski, N. M. Long, M. Nishino, W. L. Denning, A. Galan-Cobo, H. Hamdi, T. Hirz, P. Tong, J. Wang, J. Rodriguez-Canales, P. A. Villalobos, E. R. Parra, N. Kalhor, L. M. Sholl, J. L. Sauter, A. A. Jungbluth, M. Mino-Kenudson, R. Azimi, Y. Y. Elamin, J. Zhang, G. C. Leonardi, F. Jiang, K. K. Wong, J. J. Lee, V. A. Papadimitrakopoulou, I. I. Wistuba, V. A. Miller, G. M. Frampton, J. D. Wolchok, A. T. Shaw, P. A. Janne, P. J. Stephens, C. M. Rudin, W. J. Geese, L. A. Albacker, J. V. Heymach, *STK11/LKB1* mutations and PD-1 inhibitor resistance in KRAS-mutant lung adenocarcinoma. *Cancer Discov.* **8**, 822–835 (2018).
13. S. Spranger, R. M. Spaapen, Y. Zha, J. Williams, Y. Meng, T. T. Ha, T. F. Gajewski, Up-regulation of PD-L1, IDO, and T_{regs} in the melanoma tumor microenvironment is driven by $CD8^+$ T cells. *Sci. Transl. Med.* **5**, 200ra116 (2013).
14. T. Tokito, K. Azuma, A. Kawahara, H. Ishii, K. Yamada, N. Matsuo, T. Kinoshita, N. Mizukami, H. Ono, M. Kage, T. Hoshino, Predictive relevance of PD-L1 expression combined with CD8+ TIL density in stage III non-small cell lung cancer patients receiving concurrent chemoradiotherapy. *Eur. J. Cancer* **55**, 7–14 (2016).
15. L. M. LaFave, V. K. Kartha, S. Ma, K. Meli, I. Del Priore, C. Lareau, S. Naranjo, P. M. K. Westcott, F. M. Duarte, V. Sankar, Z. Chiang, A. Brack, T. Law, H. Hauck, A. Okimoto, A. Regev, J. D. Buenrostro, T. Jacks, Epigenomic state transitions characterize tumor progression in mouse lung adenocarcinoma. *Cancer Cell* **38**, 212–228.e13 (2020).
16. T. M. Gierahn, M. H. Wadsworth II, T. K. Hughes, B. D. Bryson, A. Butler, R. Satija, S. Fortune, J. C. Love, A. K. Shalek, Seq-Well: Portable, low-cost RNA sequencing of single cells at high throughput. *Nat. Methods* **14**, 395–398 (2017).
17. M. M. Gubin, X. Zhang, H. Schuster, E. Caron, J. P. Ward, T. Noguchi, Y. Ivanova, J. Hundal, C. D. Arthur, W. J. Krebber, G. E. Mulder, M. Toebes, M. D. Vesely, S. S. Lam, A. J. Korman, J. P. Allison, G. J. Freeman, A. H. Sharpe, E. L. Pearce, T. N. Schumacher, R. Aebersold, H. G. Rammensee, C. J. Melief, E. R. Mardis, W. E. Gillanders, M. N. Artyomov, R. D. Schreiber, Checkpoint blockade cancer immunotherapy targets tumour-specific mutant antigens. *Nature* **515**, 577–581 (2014).
18. H. Matsushita, M. D. Vesely, D. C. Koboldt, C. G. Rickert, R. Uppaluri, V. J. Magrini, C. D. Arthur, J. M. White, Y. S. Chen, L. K. Shea, J. Hundal, M. C. Wendl, R. Demeter, T. Wylie,

J. P. Allison, M. J. Smyth, L. J. Old, E. R. Mardis, R. D. Schreiber, Cancer exome analysis reveals a T-cell-dependent mechanism of cancer immunoediting. *Nature* **482**, 400–404 (2012).
19. J. B. Williams, B. L. Horton, Y. Zheng, Y. Duan, J. D. Powell, T. F. Gajewski, The EGR2 targets LAG-3 and 4-1BB describe and regulate dysfunctional antigen-specific CD8+ T cells in the tumor microenvironment. *J. Exp. Med.* **214**, 381–400 (2017).
20. C. E. Chibueze, M. Yoshimitsu, N. Arima, CD160 expression defines a uniquely exhausted subset of T lymphocytes in HTLV-1 infection. *Biochem. Biophys. Res. Commun.* **453**, 379–384 (2014).
21. S. R. Woo, M. E. Turnis, M. V. Goldberg, J. Bankoti, M. Selby, C. J. Nirschl, M. L. Bettini, D. M. Gravano, P. Vogel, C. L. Liu, S. Tangsombatvisit, J. F. Grosso, G. Netto, M. P. Smeltzer, A. Chaux, P. J. Utz, C. J. Workman, D. M. Pardoll, A. J. Korman, C. G. Drake, D. A. Vignali, Immune inhibitory molecules LAG-3 and PD-1 synergistically regulate T-cell function to promote tumoral immune escape. *Cancer Res.* **72**, 917–927 (2012).
22. K. Sakuishi, L. Apetoh, J. M. Sullivan, B. R. Blazar, V. K. Kuchroo, A. C. Anderson, Targeting Tim-3 and PD-1 pathways to reverse T cell exhaustion and restore anti-tumor immunity. *J. Exp. Med.* **207**, 2187–2194 (2010).
23. E. Galkina, J. Thatte, V. Dabak, M. B. Williams, K. Ley, T. J. Braciale, Preferential migration of effector CD8+ T cells into the interstitium of the normal lung. *J. Clin. Invest.* **115**, 3473–3483 (2005).
24. M. Grau, S. Valsesia, J. Mafille, S. Djebali, M. Tomkowiak, A. L. Mathieu, D. Laubreton, S. de Bernard, P. E. Jouve, E. Ventre, L. Buffat, T. Walzer, Y. Leverrier, J. Marvel, Antigen-induced but not innate memory CD8 T cells express NKG2D and are recruited to the lung parenchyma upon viral infection. *J. Immunol.* **200**, 3635–3646 (2018).
25. S. J. Ray, S. N. Franki, R. H. Pierce, S. Dimitrova, V. Koteliansky, A. G. Sprague, P. C. Doherty, A. R. de Fougerolles, D. J. Topham, The collagen binding alpha1beta1 integrin VLA-1 regulates CD8 T cell-mediated immune protection against heterologous influenza infection. *Immunity* **20**, 167–179 (2004).
26. J. Eberlein, B. Davenport, T. T. Nguyen, F. Victorino, K. Jhun, V. van der Heide, M. Kuleshov, A. Ma'ayan, R. Kedl, D. Homann, Chemokine signatures of pathogen-specific T cells I: Effector T cells. *J. Immunol.* **205**, 2169–2187 (2020).
27. B. G. Dorner, A. Scheffold, M. S. Rolph, M. B. Huser, S. H. Kaufmann, A. Radbruch, I. E. Flesch, R. A. Kroczek, MIP-1α, MIP-1β, RANTES, and ATAC/lymphotactin function together with IFN-γ as type 1 cytokines. *Proc. Natl. Acad. Sci. U.S.A.* **99**, 6181–6186 (2002).
28. S. M. Kaech, J. T. Tan, E. J. Wherry, B. T. Konieczny, C. D. Surh, R. Ahmed, Selective expression of the interleukin 7 receptor identifies effector CD8 T cells that give rise to long-lived memory cells. *Nat. Immunol.* **4**, 1191–1198 (2003).
29. C. M. Carlson, B. T. Endrizzi, J. Wu, X. Ding, M. A. Weinreich, E. R. Walsh, M. A. Wani, J. B. Lingrel, K. A. Hogquist, S. C. Jameson, Kruppel-like factor 2 regulates thymocyte and T-cell migration. *Nature* **442**, 299–302 (2006).
30. J. Rivera, R. L. Proia, A. Olivera, The alliance of sphingosine-1-phosphate and its receptors in immunity. *Nat. Rev. Immunol.* **8**, 753–763 (2008).
31. G. T. Hart, K. A. Hogquist, S. C. Jameson, Krüppel-like factors in lymphocyte biology. *J. Immunol.* **188**, 521–526 (2012).
32. T. Honda, J. G. Egen, T. Lammermann, W. Kastenmuller, P. Torabi-Parizi, R. N. Germain, Tuning of antigen sensitivity by T cell receptor-dependent negative feedback controls T cell effector function in inflamed tissues. *Immunity* **40**, 235–247 (2014).
33. T. K. Hughes, M. H. Wadsworth II, T. M. Gierahn, T. Do, D. Weiss, P. R. Andrade, F. Ma, B. J. de Andrade Silva, S. Shao, L. C. Tsoi, J. Ordovas-Montanes, J. E. Gudjonsson, R. L. Modlin, J. C. Love, A. K. Shalek, Second-strand synthesis-based massively parallel scRNA-Seq reveals cellular states and molecular features of human inflammatory skin pathologies. *Immunity* **53**, 878–894.e7 (2020).
34. H. Huang, C. Wang, F. Rubelt, T. J. Scriba, M. M. Davis, Analyzing the Mycobacterium tuberculosis immune response by T-cell receptor clustering with GLIPH2 and genome-wide antigen screening. *Nat. Biotechnol.* **38**, 1194–1202 (2020).
35. M. D. Stegall, M. Elices, G. Shepard, C. Gup, D. Ninova, D. Ferguson, R. G. Gill, The 2C T-cell transgenic mouse: An in vivo model of allospecific cytotoxic T-cell activation and homing. *Transplant. Proc.* **31**, 779 (1999).
36. Z. Chen, Z. Ji, S. F. Ngiow, S. Manne, Z. Cai, A. C. Huang, J. Johnson, R. P. Staupe, B. Bengsch, C. Xu, S. Yu, M. Kurachi, R. S. Herati, L. A. Vella, A. E. Baxter, J. E. Wu, O. Khan, J.-C. Beltra, J. R. Giles, E. Stelekati, L. M. McLane, C. W. Lau, X. Yang, S. L. Berger, G. Vahedi, H. Ji, E. J. Wherry, TCF-1-centered transcriptional network drives an effector versus exhausted CD8 T cell-fate decision. *Immunity* **51**, 840–855.e5 (2019).
37. W. H. Hudson, J. Gensheimer, M. Hashimoto, A. Wieland, R. M. Valanparambil, P. Li, J. X. Lin, B. T. Konieczny, S. J. Im, G. J. Freeman, W. J. Leonard, H. T. Kissick, R. Ahmed, Proliferating transitory T cells with an effector-like transcriptional signature emerge from PD-1$^+$ stem-like CD8$^+$ T cells during chronic infection. *Immunity* **51**, 1043–1058.e4 (2019).
38. V. Kalia, S. Sarkar, S. Subramaniam, W. N. Haining, K. A. Smith, R. Ahmed, Prolonged interleukin-2Ralpha expression on virus-specific CD8+ T cells favors terminal-effector differentiation in vivo. *Immunity* **32**, 91–103 (2010).
39. M. E. Pipkin, J. A. Sacks, F. Cruz-Guilloty, M. G. Lichtenheld, M. J. Bevan, A. Rao, Interleukin-2 and inflammation induce distinct transcriptional programs that promote the differentiation of effector cytolytic T cells. *Immunity* **32**, 79–90 (2010).
40. B. C. Miller, D. R. Sen, R. Al Abosy, K. Bi, Y. V. Virkud, M. W. LaFleur, K. B. Yates, A. Lako, K. Felt, G. S. Naik, M. Manos, E. Gjini, J. R. Kuchroo, J. J. Ishizuka, J. L. Collier, G. K. Griffin, S. Maleri, D. E. Comstock, S. A. Weiss, F. D. Brown, A. Panda, M. D. Zimmer, R. T. Manguso, F. S. Hodi, S. J. Rodig, A. H. Sharpe, W. N. Haining, Subsets of exhausted CD8(+) T cells differentially mediate tumor control and respond to checkpoint blockade. *Nat. Immunol.* **20**, 326–336 (2019).
41. A. C. Scott, F. Dundar, P. Zumbo, S. S. Chandran, C. A. Klebanoff, M. Shakiba, P. Trivedi, L. Menocal, H. Appleby, S. Camara, D. Zamarin, T. Walther, A. Snyder, M. R. Femia, E. A. Comen, H. Y. Wen, M. D. Hellmann, N. Anandasabapathy, Y. Liu, N. K. Altorki, P. Lauer, O. Levy, M. S. Glickman, J. Kaye, D. Betel, M. Philip, A. Schietinger, TOX is a critical regulator of tumour-specific T cell differentiation. *Nature* **571**, 270–274 (2019).
42. F. Alfei, K. Kanev, M. Hofmann, M. Wu, H. E. Ghoneim, P. Roelli, D. T. Utzschneider, M. von Hoesslin, J. G. Cullen, Y. Fan, V. Eisenberg, D. Wohlleber, K. Steiger, D. Merkler, M. Delorenzi, P. A. Knolle, C. J. Cohen, R. Thimme, B. Youngblood, D. Zehn, TOX reinforces the phenotype and longevity of exhausted T cells in chronic viral infection. *Nature* **571**, 265–269 (2019).
43. O. Khan, J. R. Giles, S. McDonald, S. Manne, S. F. Ngiow, K. P. Patel, M. T. Werner, A. C. Huang, K. A. Alexander, J. E. Wu, J. Attanasio, P. Yan, S. M. George, B. Bengsch, R. P. Staupe, G. Donahue, W. Xu, R. K. Amaravadi, X. Xu, G. C. Karakousis, T. C. Mitchell, L. M. Schuchter, J. Kaye, S. L. Berger, E. J. Wherry, TOX transcriptionally and epigenetically programs CD8(+) T cell exhaustion. *Nature* **571**, 211–218 (2019).
44. R. Roychoudhuri, R. L. Eil, D. Clever, C. A. Klebanoff, M. Sukumar, F. M. Grant, Z. Yu, G. Mehta, H. Liu, P. Jin, Y. Ji, D. C. Palmer, J. H. Pan, A. Chichura, J. G. Crompton, S. J. Patel, D. Stroncek, E. Wang, F. M. Marincola, K. Okkenhaug, L. Gattinoni, N. P. Restifo, The transcription factor BACH2 promotes tumor immunosuppression. *J. Clin. Invest.* **126**, 599–604 (2016).
45. M. K. Ruhland, E. W. Roberts, E. Cai, A. M. Mujal, K. Marchuk, C. Beppler, D. Nam, N. K. Serwas, M. Binnewies, M. F. Krummel, Visualizing synaptic transfer of tumor antigens among dendritic cells. *Cancer Cell* **37**, 786–799.e5 (2020).
46. E. W. Roberts, M. L. Broz, M. Binnewies, M. B. Headley, A. E. Nelson, D. M. Wolf, T. Kaisho, D. Bogunovic, N. Bhardwaj, M. F. Krummel, Critical role for CD103(+)/CD141(+) dendritic cells bearing CCR7 for tumor antigen trafficking and priming of T cell immunity in melanoma. *Cancer Cell* **30**, 324–336 (2016).
47. D. T. Utzschneider, S. S. Gabriel, D. Chisanga, R. Gloury, P. M. Gubser, A. Vasanthakumar, W. Shi, A. Kallies, Early precursor T cells establish and propagate T cell exhaustion in chronic infection. *Nat. Immunol.* **21**, 1256–1266 (2020).
48. M. Sade-Feldman, K. Yizhak, S. L. Bjorgaard, J. P. Ray, C. G. de Boer, R. W. Jenkins, D. J. Lieb, J. H. Chen, D. T. Frederick, M. Barzily-Rokni, S. S. Freeman, A. Reuben, P. J. Hoover, A. C. Villani, E. Ivanova, A. Portell, P. H. Lizotte, A. R. Aref, J. P. Eliane, M. R. Hammond, H. Vitzthum, S. M. Blackmon, B. Li, V. Gopalakrishnan, S. M. Reddy, Z. A. Cooper, C. P. Paweletz, D. A. Barbie, A. Stemmer-Rachamimov, K. T. Flaherty, J. A. Wargo, G. M. Boland, R. J. Sullivan, G. Getz, N. Hacohen, Defining T cell states associated with response to checkpoint immunotherapy in melanoma. *Cell* **175**, 998–1013.e20 (2018).
49. S. Kurtulus, A. Madi, G. Escobar, M. Klapholz, J. Nyman, E. Christian, M. Pawlak, D. Dionne, J. Xia, O. Rozenblatt-Rosen, V. K. Kuchroo, A. Regev, A. C. Anderson, Checkpoint blockade immunotherapy induces dynamic changes in PD-1$^-$CD8$^+$ tumor-infiltrating T cells. *Immunity* **50**, 181–194.e6 (2019).
50. C. S. Jansen, N. Prokhnevska, V. A. Master, M. G. Sanda, J. W. Carlisle, M. A. Bilen, M. Cardenas, S. Wilkinson, R. Lake, A. G. Sowalsky, R. M. Valanparambil, W. H. Hudson, D. McGuire, K. Melnick, A. I. Khan, K. Kim, Y. M. Chang, A. Kim, C. P. Filson, M. Alemozaffar, A. O. Osunkoya, P. Mullane, C. Ellis, R. Akondy, S. J. Im, A. O. Kamphorst, A. Reyes, Y. Liu, H. Kissick, An intra-tumoral niche maintains and differentiates stem-like CD8 T cells. *Nature* **576**, 465–470 (2019).
51. S. J. Im, M. Hashimoto, M. Y. Gerner, J. Lee, H. T. Kissick, M. C. Burger, Q. Shan, J. S. Hale, J. Lee, T. H. Nasti, A. H. Sharpe, G. J. Freeman, R. N. Germain, H. I. Nakaya, H. H. Xue, R. Ahmed, Defining CD8+ T cells that provide the proliferative burst after PD-1 therapy. *Nature* **537**, 417–421 (2016).
52. M. V. Kim, W. Ouyang, W. Liao, M. Q. Zhang, M. O. Li, Murine in vivo CD8$^+$ T cell killing assay. *Bio Protoc.* **4**, e1172 (2014).
53. P. Gueguen, C. Metoikidou, T. Dupic, M. Lawand, C. Goudot, S. Baulande, S. Lameiras, O. Lantz, N. Girard, A. Seguin-Givelet, M. Lefevre, T. Mora, A. M. Walczak, J. J. Waterfall, S. Amigorena, Contribution of resident and circulating precursors to tumor-infiltrating CD8$^+$ T cell populations in lung cancer. *Sci. Immunol.* **6**, eabd5778 (2021).
54. X. Guo, Y. Zhang, L. Zheng, C. Zheng, J. Song, Q. Zhang, B. Kang, Z. Liu, L. Jin, R. Xing, R. Gao, L. Zhang, M. Dong, X. Hu, X. Ren, D. Kirchhoff, H. G. Roider, T. Yan, Z. Zhang, Global characterization of T cells in non-small-cell lung cancer by single-cell sequencing. *Nat. Med.* **24**, 978–985 (2018).

55. A. M. Laughney, J. Hu, N. R. Campbell, S. F. Bakhoum, M. Setty, V. P. Lavallee, Y. Xie, I. Masilionis, A. J. Carr, S. Kottapalli, V. Allaj, M. Mattar, N. Rekhtman, J. B. Xavier, L. Mazutis, J. T. Poirier, C. M. Rudin, D. Pe'er, J. Massague, Regenerative lineages and immune-mediated pruning in lung cancer metastasis. *Nat. Med.* **26**, 259–269 (2020).
56. R. Zilionis, C. Engblom, C. Pfirschke, V. Savova, D. Zemmour, H. D. Saatcioglu, I. Krishnan, G. Maroni, C. V. Meyerovitz, C. M. Kerwin, S. Choi, W. G. Richards, A. De Rienzo, D. G. Tenen, R. Bueno, E. Levantini, M. J. Pittet, A. M. Klein, Single-cell transcriptomics of human and mouse lung cancers reveals conserved myeloid populations across individuals and species. *Immunity* **50**, 1317–1334.e10 (2019).
57. N. Momin, N. K. Mehta, N. R. Bennett, L. Ma, J. R. Palmeri, M. M. Chinn, E. A. Lutz, B. Kang, D. J. Irvine, S. Spranger, K. D. Wittrup, Anchoring of intratumorally administered cytokines to collagen safely potentiates systemic cancer immunotherapy. *Sci. Transl. Med.* **11**, eaaw2614 (2019).
58. E. F. Zhu, S. A. Gai, C. F. Opel, B. H. Kwan, R. Surana, M. C. Mihm, M. J. Kauke, K. D. Moynihan, A. Angelini, R. T. Williams, M. T. Stephan, J. S. Kim, M. B. Yaffe, D. J. Irvine, L. M. Weiner, G. Dranoff, K. D. Wittrup, Synergistic innate and adaptive immune response to combination immunotherapy with anti-tumor antigen antibodies and extended serum half-life IL-2. *Cancer Cell* **27**, 489–501 (2015).
59. J. Clarke, B. Panwar, A. Madrigal, D. Singh, R. Gujar, O. Wood, S. J. Chee, S. Eschweiler, E. V. King, A. S. Awad, C. J. Hanley, K. J. McCann, S. Bhattacharyya, E. Woo, A. Alzetani, G. Seumois, G. J. Thomas, A. P. Ganesan, P. S. Friedmann, T. Sanchez-Elsner, F. Ay, C. H. Ottensmeier, P. Vijayanand, Single-cell transcriptomic analysis of tissue-resident memory T cells in human lung cancer. *J. Exp. Med.* **216**, 2128–2149 (2019).
60. S. Corgnac, I. Malenica, L. Mezquita, E. Auclin, E. Voilin, J. Kacher, H. Halse, L. Grynszpan, N. Signolle, T. Dayris, M. Leclerc, N. Droin, V. de Montpreville, O. Mercier, P. Validire, J. Y. Scoazec, C. Massard, S. Chouaib, D. Planchard, J. Adam, B. Besse, F. Mami-Chouaib, CD103(+)CD8(+) TRM cells accumulate in tumors of anti–PD-1-responder lung cancer patients and are tumor-reactive lymphocytes enriched with Tc17. *Cell Rep Med.* **1**, 100127 (2020).
61. A. P. Ganesan, J. Clarke, O. Wood, E. M. Garrido-Martin, S. J. Chee, T. Mellows, D. Samaniego-Castruita, D. Singh, G. Seumois, A. Alzetani, E. Woo, P. S. Friedmann, E. V. King, G. J. Thomas, T. Sanchez-Elsner, P. Vijayanand, C. H. Ottensmeier, Tissue-resident memory features are linked to the magnitude of cytotoxic T cell responses in human lung cancer. *Nat. Immunol.* **18**, 940–950 (2017).
62. D. S. Thommen, V. H. Koelzer, P. Herzig, A. Roller, M. Trefny, S. Dimeloe, A. Kiialainen, J. Hanhart, C. Schill, C. Hess, S. Savic Prince, M. Wiese, D. Lardinois, P. C. Ho, C. Klein, V. Karanikas, K. D. Mertz, T. N. Schumacher, A. Zippelius, A transcriptionally and functionally distinct PD-1(+) CD8(+) T cell pool with predictive potential in non-small-cell lung cancer treated with PD-1 blockade. *Nat. Med.* **24**, 994–1004 (2018).
63. M. DuPage, C. Mazumdar, L. M. Schmidt, A. F. Cheung, T. Jacks, Expression of tumour-specific antigens underlies cancer immunoediting. *Nature* **482**, 405–409 (2012).
64. A. Schietinger, J. J. Delrow, R. S. Basom, J. N. Blattman, P. D. Greenberg, Rescued tolerant CD8 T cells are preprogrammed to reestablish the tolerant state. *Science* **335**, 723–727 (2012).
65. H. M. Shin, G. Kim, S. Kim, J. H. Sim, J. Choi, M. Kim, M. Kwon, S. K. Ye, D. S. Lee, S. W. Cho, S. T. Kim, J. Lee, H. R. Kim, Chromatin accessibility of circulating CD8(+) T cells predicts treatment response to PD-1 blockade in patients with gastric cancer. *Nat. Commun.* **12**, 975 (2021).
66. T. Sekine, A. Perez-Potti, S. Nguyen, J. B. Gorin, V. H. Wu, E. Gostick, S. Llewellyn-Lacey, Q. Hammer, S. Falck-Jones, S. Vangeti, M. Yu, A. Smed-Sorensen, A. Gaballa, M. Uhlin, J. K. Sandberg, C. Brander, P. Nowak, P. A. Goepfert, D. A. Price, M. R. Betts, M. Buggert, TOX is expressed by exhausted and polyfunctional human effector memory $CD8^+$ T cells. *Sci. Immunol.* **5**, eaba7918 (2020).
67. F. Baharom, R. A. Ramirez-Valdez, K. K. S. Tobin, H. Yamane, C. A. Dutertre, A. Khalilnezhad, G. V. Reynoso, V. L. Coble, G. M. Lynn, M. P. Mule, A. J. Martins, J. P. Finnigan, X. M. Zhang, J. A. Hamerman, N. Bhardwaj, J. S. Tsang, H. D. Hickman, F. Ginhoux, A. S. Ishizuka, R. A. Seder, Intravenous nanoparticle vaccination generates stem-like TCF1(+) neoantigen-specific CD8(+) T cells. *Nat. Immunol.* **22**, 41–52 (2021).
68. A. Li, R. H. Herbst, D. Canner, J. M. Schenkel, O. C. Smith, J. Y. Kim, M. Hillman, A. Bhutkar, M. S. Cuoco, C. G. Rappazzo, P. Rogers, C. Dang, L. Jerby-Arnon, O. Rozenblatt-Rosen, L. Cong, M. Birnbaum, A. Regev, T. Jacks, IL-33 signaling alters regulatory T Cell diversity in support of tumor development. *Cell Rep.* **29**, 2998–3008.e8 (2019).
69. M. Casanova-Acebes, E. Dalla, A. M. Leader, J. LeBerichel, J. Nikolic, B. M. Morales, M. Brown, C. Chang, L. Troncoso, S. T. Chen, A. Sastre-Perona, M. D. Park, A. Tabachnikova, M. Dhainaut, P. Hamon, B. Maier, C. M. Sawai, E. Agullo-Pascual, M. Schober, B. D. Brown, B. Reizis, T. Marron, E. Kenigsberg, C. Moussion, P. Benaroch, J. A. Aguirre-Ghiso, M. Merad, Tissue-resident macrophages provide a pro-tumorigenic niche to early NSCLC cells. *Nature* **595**, 578–584 (2021).
70. T. Barthlott, H. Moncrieffe, M. Veldhoen, C. J. Atkins, J. Christensen, A. O'Garra, B. Stockinger, CD25+ CD4+ T cells compete with naive CD4+ T cells for IL-2 and exploit it for the induction of IL-10 production. *Int. Immunol.* **17**, 279–288 (2005).
71. T. Chinen, A. K. Kannan, A. G. Levine, X. Fan, U. Klein, Y. Zheng, G. Gasteiger, Y. Feng, J. D. Fontenot, A. Y. Rudensky, An essential role for the IL-2 receptor in Treg cell function. *Nat. Immunol.* **17**, 1322–1333 (2016).
72. J. D. Leonard, D. C. Gilmore, T. Dileepan, W. I. Nawrocka, J. L. Chao, M. H. Schoenbach, M. K. Jenkins, E. J. Adams, P. A. Savage, Identification of natural regulatory T cell epitopes reveals convergence on a dominant autoantigen. *Immunity* **47**, 107–117.e8 (2017).
73. S. Malchow, D. S. Leventhal, S. Nishi, B. I. Fischer, L. Shen, G. P. Paner, A. S. Amit, C. Kang, J. E. Geddes, J. P. Allison, N. D. Socci, P. A. Savage, Aire-dependent thymic development of tumor-associated regulatory T cells. *Science* **339**, 1219–1224 (2013).
74. G. Trinchieri, Interleukin-12 and the regulation of innate resistance and adaptive immunity. *Nat. Rev. Immunol.* **3**, 133–146 (2003).
75. C. S. Garris, S. P. Arlauckas, R. H. Kohler, M. P. Trefny, S. Garren, C. Piot, C. Engblom, C. Pfirschke, M. Siwicki, J. Gungabeesoon, G. J. Freeman, S. E. Warren, S. Ong, E. Browning, C. G. Twitty, R. H. Pierce, M. H. Le, A. P. Algazi, A. I. Daud, S. I. Pai, A. Zippelius, R. Weissleder, M. J. Pittet, Successful Anti–PD-1 cancer immunotherapy requires T cell-dendritic cell crosstalk involving the cytokines IFN-γ and IL-12. *Immunity* **49**, 1148–1161.e7 (2018).
76. C. N. Skon, J. Y. Lee, K. G. Anderson, D. Masopust, K. A. Hogquist, S. C. Jameson, Transcriptional downregulation of S1pr1 is required for the establishment of resident memory CD8+ T cells. *Nat. Immunol.* **14**, 1285–1293 (2013).
77. C. R. Glassman, Y. K. Mathiharan, K. M. Jude, L. Su, O. Panova, P. J. Lupardus, J. B. Spangler, L. K. Ely, C. Thomas, G. Skiniotis, K. C. Garcia, Structural basis for IL-12 and IL-23 receptor sharing reveals a gateway for shaping actions on T versus NK cells. *Cell* **184**, 983–999.e24 (2021).
78. N. S. Joshi, E. H. Akama-Garren, Y. Lu, D. Y. Lee, G. P. Chang, A. Li, M. DuPage, T. Tammela, N. R. Kerper, A. F. Farago, R. Robbins, D. M. Crowley, R. T. Bronson, T. Jacks, Regulatory T cells in tumor-associated tertiary lymphoid structures suppress anti-tumor T cell responses. *Immunity* **43**, 579–590 (2015).
79. J. Schindelin, I. Arganda-Carreras, E. Frise, V. Kaynig, M. Longair, T. Pietzsch, S. Preibisch, C. Rueden, S. Saalfeld, B. Schmid, J. Y. Tinevez, D. J. White, V. Hartenstein, K. Eliceiri, P. Tomancak, A. Cardona, Fiji: An open-source platform for biological-image analysis. *Nat. Methods* **9**, 676–682 (2012).
80. E. Z. Macosko, A. Basu, R. Satija, J. Nemesh, K. Shekhar, M. Goldman, I. Tirosh, A. R. Bialas, N. Kamitaki, E. M. Martersteck, J. J. Trombetta, D. A. Weitz, J. R. Sanes, A. K. Shalek, A. Regev, S. A. McCarroll, Highly parallel genome-wide expression profiling of individual cells using nanoliter droplets. *Cell* **161**, 1202–1214 (2015).
81. V. K. Mootha, C. M. Lindgren, K. F. Eriksson, A. Subramanian, S. Sihag, J. Lehar, P. Puigserver, E. Carlsson, M. Ridderstrale, E. Laurila, N. Houstis, M. J. Daly, N. Patterson, J. P. Mesirov, T. R. Golub, P. Tamayo, B. Spiegelman, E. S. Lander, J. N. Hirschhorn, D. Altshuler, L. C. Groop, PGC-1alpha-responsive genes involved in oxidative phosphorylation are coordinately downregulated in human diabetes. *Nat. Genet.* **34**, 267–273 (2003).
82. A. Subramanian, P. Tamayo, V. K. Mootha, S. Mukherjee, B. L. Ebert, M. A. Gillette, A. Paulovich, S. L. Pomeroy, T. R. Golub, E. S. Lander, J. P. Mesirov, Gene set enrichment analysis: A knowledge-based approach for interpreting genome-wide expression profiles. *Proc. Natl. Acad. Sci. U.S.A.* **102**, 15545–15550 (2005).
83. A. Butler, P. Hoffman, P. Smibert, E. Papalexi, R. Satija, Integrating single-cell transcriptomic data across different conditions, technologies, and species. *Nat. Biotechnol.* **36**, 411–420 (2018).
84. A. A. Tu, T. M. Gierahn, B. Monian, D. M. Morgan, N. K. Mehta, B. Ruiter, W. G. Shreffler, A. K. Shalek, J. C. Love, TCR sequencing paired with massively parallel 3' RNA-seq reveals clonotypic T cell signatures. *Nat. Immunol.* **20**, 1692–1699 (2019).
85. J. A. Vander Heiden, G. Yaari, M. Uduman, J. N. Stern, K. C. O'Connor, D. A. Hafler, F. Vigneault, S. H. Kleinstein, pRESTO: A toolkit for processing high-throughput sequencing raw reads of lymphocyte receptor repertoires. *Bioinformatics* **30**, 1930–1932 (2014).
86. N. T. Gupta, J. A. Vander Heiden, M. Uduman, D. Gadala-Maria, G. Yaari, S. H. Kleinstein, Change-O: A toolkit for analyzing large-scale B cell immunoglobulin repertoire sequencing data. *Bioinformatics* **31**, 3356–3358 (2015).
87. T. Stuart, A. Butler, P. Hoffman, C. Hafemeister, E. Papalexi, W. M. Mauck III, Y. Hao, M. Stoeckius, P. Smibert, R. Satija, Comprehensive integration of single-cell data. *Cell* **177**, 1888–1902.e21 (2019).
88. L. Haghverdi, M. Buttner, F. A. Wolf, F. Buettner, F. J. Theis, Diffusion pseudotime robustly reconstructs lineage branching. *Nat. Methods* **13**, 845–848 (2016).
89. F. A. Wolf, P. Angerer, F. J. Theis, SCANPY: Large-scale single-cell gene expression data analysis. *Genome Biol.* **19**, 15 (2018).

Acknowledgments: We would like to thank M. Duquette for technical assistance and the Koch Institute's Robert A. Swanson (1969) Biotechnology Center for technical support, specifically the Flow Cytometry, Histology, and Preclinical Imaging and Testing facilities. **Funding:** S.S. was funded by the Pew-Stewart Scholars for Cancer Research. B.L.H. was funded by a Ludwig Center for Molecular Oncology Post-Doctoral Fellowship. S.S. and J.C.L. were

funded by the Koch Institute Frontier Research Program through the Casey and Family Foundation Cancer Research Fund. This work was supported by the Koch Institute Support Grant P30-CA14051 from the National Cancer Institute. **Author contributions:** B.L.H. and S.S. conceptualized the study. B.L.H. and D.M.M. performed data curation. B.L.H., D.M.M., M.Z., V.B., and E.T.-M. performed formal analysis of data. B.L.H., J.C.L., and S.S. acquired funding. B.L.H. and D.M.M. developed methodology. B.L.H., D.M.M., M.Z., V.B., and E.T.-M. performed investigation. B.L.H., D.M.M., and S.S. created the data visualization. B.L.H. and S.S. performed project administration. N.M. and K.D.W. donated resources. D.M.M., M.Z., and V.B. used and developed software. J.C.L. and S.S. provided supervision. B.L.H., D.M.M., and S.S. wrote the original draft. B.L.H., D.M.M., S.S., J.C.L., and M.Z. reviewed and edited the manuscript. **Competing interests:** S.S. is a SAB member for Arcus Biosciences and Venn Therapeutics. S.S. is a consultant for TAKEDA, Merck, Tango Therapeutics, and Ribon Therapeutics and received funding for unrelated projects from Exelicis and TAKEDA. J.C.L. has interests in Sunflower Therapeutics PBC, Pfizer, Honeycomb Biotechnologies, OneCyte Biotechnologies, SQZ Biotechnologies, Alloy Therapeutics, QuantumCyte, Amgen, and Repligen. J.C.L.'s interests are reviewed and managed under MIT's policies for potential conflicts of interest. J.C.L. receives sponsored research support at MIT from Amgen, the Bill & Melinda Gates Foundation, Biogen, Pfizer, Roche, Takeda, and Sanofi. B.L.H., D.M.M., K.D.W., J.C.L., and S.S. are inventors on patent application 63/158,225 submitted by the MIT that covers lung cancer–specific T cell dysfunction. **Data and materials availability:** All data and materials are available upon request from the corresponding author. Sequencing data can be found in the GEO database under accession number GSE184388. All data needed to evaluate the conclusions in the paper are present in the paper or the Supplementary Materials.

Submitted 6 April 2021
Resubmitted 9 August 2021
Accepted 21 September 2021
Published 29 October 2021
10.1126/sciimmunol.abi8800

Citation: B. L. Horton, D. M. Morgan, N. Momin, M. Zagorulya, E. Torres-Mejia, V. Bhandarkar, K. D. Wittrup, J. C. Love, S. Spranger, Lack of $CD8^+$ T cell effector differentiation during priming mediates checkpoint blockade resistance in non–small cell lung cancer. *Sci. Immunol.* **6**, eabi8800 (2021).

Science Immunology

Lack of CD8 T cell effector differentiation during priming mediates checkpoint blockade resistance in non–small cell lung cancer

Brendan L. HortonDuncan M. MorganNoor MominMaria ZagorulyaElen Torres-MejiaVidit BhandarkarK. Dane WittrupJ. Christopher LoveStefani Spranger

Sci. Immunol., 6 (64), eabi8800. • DOI: 10.1126/sciimmunol.abi8800

A unique T cell subset in lung cancer
Although some non–small cell lung cancers (NSCLC) are sensitive to immune checkpoint blockade (ICB), many patients with NSCLC do not respond to ICB, which may relate to the lack of infiltration of CD8 T cells. Here, Horton *et al.* used mouse models of flank and lung tumors to show that CD8 T cells from lung tumors, not flank tumors, had a dysfunctional phenotype distinct from conventional T cell exhaustion that was established in the draining lymph node and correlated to ICB resistance. IL-2 and IL-12 treatment rescued this phenotype, leading to control of lung tumors. These data suggest that cytokine therapy might be able to rescue a specific subset of dysfunctional T cells found in lung tumors.